**Charles University**

**Faculty of Science**

Study programme: Genetics, Molecular Biology and Virology

Branch of study: N-GEMOEU


**Bc. Yuliia Arishaka**

# Identification of new tissue-specific interaction partners of chromatin remodelling ATPase Smarca5

# Identifikace nových tkáňově specifických interakčních partnerů chromatin remodelační ATPázy Smarca5

Diploma thesis

Supervisor: Mgr. Juraj Kokavec, Ph.D.

Prague, 2024

**Prohlášení:**

Prohlašuji, že jsem závěrečnou práci zpracovala samostatně a že jsem uvedla všechny použité informační zdroje a literaturu. Tato práce ani její podstatná část nebyla předložena k získání jiného nebo stejného akademického titulu.

V Praze, 01.04.2024

Arishaka Yuliia

**Acknowledgment:**

I would like to express my heartfelt gratitude to my supervisor, Juraj Kokavec, Ph.D., for his unwavering support, endless patience, and remarkable dedication throughout this project. His guidance and commitment have been crucial to the advancements made in this research. I am also grateful to prof. MUDr. Tomáš Stopka, Ph.D., for his invaluable mentorship and guidance. Additionally, I am deeply thankful to Lukáš Čermák, Ph.D and Alikhan Abdirov, M.Sc., from the Laboratory of Cancer Biology at Institute of Molecular Genetics of the Czech Academy of Sciences for their expert help with biochemistry methods and to Pavel Talacko, M.Sc., from the Laboratory of Mass Spectrometry at BIOCEV, who helped with mass spectrometric analyses, which greatly enhanced the quality and depth of this thesis. This work was made possible through the generous support of the Agency of the Czech Ministry of Health (NU22-05-00374, NU21-08-00312), Charles University Grants (UNCE/MED/016, Cooperatio, SVV260521), and the Next Generation EU Programme EXCELES (LX22NPO5102).

# Abstrakt

Regulace struktury chromatinu je zásadní pro širokou škálu buněčných procesů, včetně regulace transkripce, buněčného dělení, diferenciace a opravy poškození DNA, a ATP-závislé remodelační komplexy chromatinu byly identifikovány jako základní složky této regulační sítě. Bylo ukázáno, že Smarca5, jako enzym ATPáza/Helikáza, reguluje strukturu chromatinu v interakci s partnery obsahujícími bromo- a DDT-WHIM domény, což umožňuje kontrolovat vazbu proteinů a transkripčních faktorů na specifické DNA sekvence spojené s chromatinem. V této práci byl identifikován dosud necharakterizovaný protein s konzervovanou N-terminální bromodoménou a ISWI protein vázající DDT-WHIM doménou pomocí ko-imunoprecipitace a hmotnostní spektrometrie v buněčných liniích savčího typu. Tento protein byl potvrzen jako nový interakční partner ATPázy pro remodelaci chromatinu, Smarca5. Navíc, byla lokalizována oblast nezbytná pro interakci se Smarca5, která odpovídá oblasti DDT-WHIM domény. Navíc jsme se pokusili identifikovat další interakční partnery, kteří by mohli naznačovat potenciální funkci tohoto nového chromatin remodelačního komplexu, a ověřili jsme jeho expresi v embryonálních a postnatálních tkáních. Tento objev představuje jedinečnou příležitost pro další zkoumání jeho potenciální role v interakci s ATPázou Smarca5 a rozšíření našeho poznání o funkcích Smarca5 v regulaci buněčné homeostázy.



**Klíčová slova**

remodelace chromatinu, Smarca5, bromodoména, western blot, ko-imunoprecipitace, hmotnostní spektroskopie

## Abstract

The regulation of chromatin structure is fundamental to a wide range of cellular processes, including transcriptional regulation, cell division, differentiation and DNA damage repair, and ATP-dependent chromatin remodeling complexes have been established as essential components of this regulatory network. Smarca5, as an ATPase/Helicase enzyme, has been shown to regulate chromatin structure by interacting with bromodomain and DDT-WHIM domain-containing partners to control the binding of chromatin-associated proteins and transcription factors to their specific DNA target sequences. In this work we identify a previously uncharacterized protein with a conserved N-terminal bromodomain and ISWI protein binding DDT-WHIM domain through co-immunoprecipitation and mass spectrometry in mammalian cell lines and establish it as a novel interaction partner of chromatin remodeling ATPase Smarca5. Furthermore, we have pinpointed the region required for Smarca5 interaction that corresponds to DDT-WHIM domain. We have furthermore attempted to identify additional interaction partners which may hint on the potential function of this novel chromatin complex and validated its expression in embryonic and postnatal tissues. This discovery represents a unique opportunity for further investigation into its potential function in interaction with ATPase Smarca5, and expansion of current roles of Smarca5 in the regulation of cell homeostasis.

**Keywords**

chromatin remodelling, Smarca5, bromodomain, western blot, co-immunoprecipitation, mass spectrometry

# Contents

# 1 Introduction

Chromatin, a complex consisting of proteins, RNA, and DNA molecules, plays a critical role in regulating various nuclear processes, including gene expression, DNA repair and replication, cell division and DNA recombination. The structural organization of chromatin is controlled by enzymes known as chromatin remodelers, which possess ATPase activity. These remodelers can perform several functions like nucleosome sliding, exchange of histone variants, ejection of nucleosomes, unwrapping of chromatin, and the assembly of nucleosomes. Additionally, these remodeler proteins often interact with other regulatory proteins, forming complexes that influence their specific roles within the cell environment itself.

Smarca5, also known as SWI/SNF Related, Matrix Associated, Actin Dependent Regulator of Chromatin, Subfamily A, Member 5, belongs to the ISWI family and acts as a chromatin remodeling factor. This ATPase plays an important role in processes such as hematopoiesis, spermatogenesis, and brain development through nucleosome spacing. Studies have shown that dysregulation of SMARCA5 expression is associated with various human malignancies, including gastric cancer, breast cancer, lung cancer, and acute leukemia.

Smarca1 (SWI/SNF Related, Matrix Associated, Actin Dependent Regulator of Chromatin, Subfamily A, Member 1) is a homolog of Smarca5 and is mainly expressed in post-mitotic neurons. Its role involves controlling cell cycle exit by modulating FoxG1 dosage to regulate neural output and cortical differentiation. Ultimately, this influences brain size by facilitating progenitor cell differentiation through gene expression regulation at the Foxg1 locus.

Smarca1 and Smarca5 form highly conserved complexes found in a wide range of organisms, including plants, fungi, and animals. One of their significant interaction partners is Cat Eye Syndrome Chromosome Region Candidate 2 (CECR2), which plays a pivotal role in both spermatogenesis and neurogenesis. This thesis aims to explore and confirm potential new interaction partners of Smarca5 - specifically previously uncharacterized protein, BRD10 (KIAA2026). Brd10 demonstrates a similar expression pattern to Smarca5 in spermatocytes and spermatogonia, as well as protein domains suggesting its potential as a novel ISWI binding partner. By investigating the interaction partners of Smarca5 in mammalian cell line models, we can gain deeper insights into the tissue-specific function of this protein and its impact on chromatin regulation.

# 2 Abbreviations

| | |
|---|---|
| ACF1 | ATP-utilizing Chromatin Assembly and Remodeling Factor 1 |
| ARP | Actin Related Proteins |
| BAZ | Bromodomain Adjacent to PHD Zinc Finger Protein |
| BRD | Bromodomain |
| BPTF | PHD Finger Transcription Factor |
| BRD10 | Bromodomain-containing 10 protein |
| (B)WICH | WSTF-ISWI Chromatin Remodeling Complex |
| CECR2 | Cat Eye Syndrome Chromosome Region Candidate 2 |
| CERF | CECR2-Containing Remodeling Factor |
| CES | Cat Eye Syndrome |
| CHD | Chromodomain Helicase DNA-Binding |
| CHD1 | Chromodomain-helicase-DNA-binding protein 1 |
| CHRAC | Chromatin Accessibility Complex |
| CSB | Cockayne syndrome protein B |
| CTCF | CCCTC-Binding Factor |
| DLX5 | Distal-Less Homeobox 5 |
| FACT | Facilitates Chromatin Transcription Complex |
| FOXG1 | Forkhead Box G1 |
| HAT | Histone Acetyltransferases |
| HDAC1 | Histone Deacetylase 1 |
| HSA | Helicase/SANT–Associated Domain |
| HSS | HAND-SANT-SLIDE domain |
| IBM-C | ISWI binding module C-terminal |
| INO80 | Inositol Requiring 80 |
| ISWI | Imitation Switch |
| MAR | Matrix-Associated Region |

| | |
|---|---|
| MBD | Methyl-CpG-Binding Domain |
| NoRC | Nucleolar Remodeling Complex |
| NuRD | Nucleosome Remodeling and Histone Deacetylation Complex |
| NURF | Nucleosome Remodelling Factor |
| PHD | Plant Homeodomain |
| RSF | Remodelling and Spacing Factor |
| SMARCA1 | SWI/SNF Related, Matrix Associated, Actin Dependent Regulator of Chromatin, Subfamily A, Member 1 |
| SMARCA5 | SWI/SNF-Related, Matrix-Associated, Actin-Dependent Regulator of Chromatin, Subfamily A, Member 5 |
| SNF2H | Sucrose Nonfermenting-2-Homolog |
| SNF2L | Sucrose Nonfermenting-2-Like |
| SWI/SNF | Switch/Sucrose Nonfermentable |
| TAM | Transient Abnormal Myelopoiesis |
| TIP5 | Transcription termination factor I-interacting protein 5 |
| TTF-I | Transcription termination factor, RNA polymerase I |
| WSTF | Williams Syndrome Transcription Factor |

# 3 Literature Review

## 3.1 ATP-dependent chromatin remodelers

Chromatin is a highly dynamic structure that can be modified by a variety of chromatin remodelers. One of the most well-studied groups of chromatin remodelers are ATP-dependent chromatin remodelers, which utilize energy from ATP hydrolysis to disrupt the contacts between histones and DNA, and thus regulate the dynamic access to the packaged DNA (Tyagi *et al*., 2016).

There are four distinct families of ATP-dependent chromatin remodelers: switch/sucrose nonfermentable (SWI/SNF), imitation SWI (ISWI), chromodomain helicase DNA-binding (CHD), and inositol requiring 80 (INO80) (Fig.1). Despite sharing a conserved ATPase domain, these families are distinguished based upon an unique flanking domains. For example, the SWI/SNF family contains bromodomain and Helicase/SANT–associated domain (HSA), the ISWI family contains SANT-SLIDE modules, the CHD family contains tandem chromodomains, and the INO80 family contains HSA domains. All ATP-dependent chromatin remodelers contain a SWI2/SNF2-family ATPase subunit, which is characterized by an ATPase domain that is split into two parts: DExx and HELICc (Clapier and Cairns, 2009).

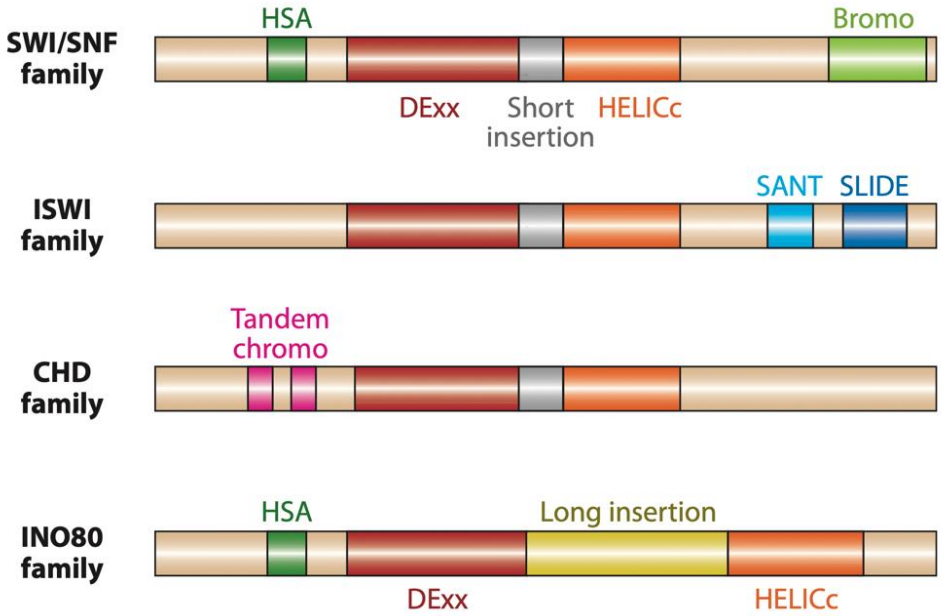


**Fig. 1 | ATP-dependent chromatin remodelers.** The SWI/SNF family is characterized by a bromodomain (light green) and an HAS domain (dark green), while the ISWI family is defined by a SANT-SLIDE domain (blue). The CHD family features tandem chromodomains (pink), and the INO80 family includes an HSA domain (dark green) and a long insertion (yellow), meanwhile other families comprise short insertion (gray) within the ATPase domain. Each remodeler family contains an ATPase domain: DExx (red) and HELICc (orange) (adapted from Clapier and Cairns, 2009).

### 3.1.1 Switching defective/sucrose non-fermenting (SWI/SNF)

Initially found in yeast, the SWI/SNF complexes were responsible for regulating the switching of mating types and activating pathways for sucrose fermentation. Subsequently, these complexes were identified as significant global regulators of transcription through ATP-dependent chromatin remodeling in both *Drosophila* and mammals. SWI/SNF are recruited to chromatin by recognizing specific post-translational modifications on histones, such as acetylation, through the bromodomain subunit present within the ATPases. Another unique feature of the SWI/SNF complexes is the presence of actin and actin related proteins (ARP), which have been proposed to play a role in modulating complex assembly and stability, DNA-dependent ATPase activity, remodeling and translocation of histones (Neigeborn and Carlson, 1984; Stern *et al*., 1984; Tamkun *et al*., 1992; Klages-Mundt *et al*., 2018).

SWI/SNF family complexes bind to various genomic loci, including distal enhancers, promoters, and CCCTC-binding factor (CTCF)-binding sites. They facilitate and maintain DNA accessibility to regulate gene transcription, making them key players in transcriptional regulation. Mammalian SWI/SNF complexes have been implicated in the control of specific transcriptional programs, such as those mediating cell differentiation and lineage specification. The significance of SWI/SNF in biological processes is further emphasized by the fact that more than 20% of human cancers carry a mutation in SWI/SNF complex subunit genes. SWI/SNF has also been shown to play a role in facilitating repair of double-strand breaks, through non-homologous end-joining and homologous recombination, and in repairing helix-distorting DNA damage through nucleotide excision repair (Ribeiro-Silva *et al*., 2019; Centore *et al*., 2020; Mittal and Roberts, 2020).

### 3.1.2 Inositol requiring 80 (INO80)

INO80 is a large, multi-subunit complex that plays a critical role in double-strand break repair. It was first identified in *Saccharomyces cerevisiae* and has been implicated in various DNA-based processes, including regulation of transcription, DNA replication, recombination, and DNA damage repair. INO80 cooperates with ISWI to correctly space the nucleosomes and has the capability to properly organize the promoter nucleosome architecture and reposition nucleosomes after their destabilization by the transcription machinery. This underscores the importance of INO80 in DNA maintenance and repair (Shen *et al*., 2000; Poli *et al*., 2017).

The unique binding mode of INO80 with nucleosomes distinguishes it from other chromatin remodelers. The interaction between INO80 and nucleosomes alters DNA

translocation mechanism and induces unwrapping of nucleosomal DNA near the nucleosome entry site. It disrupts DNA-histone interactions to partially expose H2AZ-H2B dimers. INO80 interacting ARPs are involved in INO80 family remodeling and play a vital role in histone recognition as they exhibit specific preferences for certain histone types. The role of INO80 in various biological processes is emphasized by its global functions, including transcriptional regulation and DNA damage repair (Shen *et al*., 2003; Reyes *et al*., 2021).

### 3.1.3 Chromodomain, Helicase, DNA binding (CHD)

CHD family is a group of nine proteins in human, each of which contains two chromodomains arranged in tandem in the N-terminal region of the ATPase/helicase domain. One unique feature of CHD proteins is their ability to coordinate with multiple chromatin-modifying complexes. Among these proteins, Chromodomain-helicase-DNA-binding protein 1 (CHD1) has been extensively studied and has been shown to play important roles in nucleosome assembly, sliding, and spacing in vitro. It has also been found to interact with several factors involved in gene transcription, as well as being required for the passage of RNA polymerase II through nucleosomes and cellular pluripotency regulation (Stanley *et al*., 2013).

The nucleosome remodeling and histone deacetylation (NuRD) complex, a vital player in various biological processes, has an extensive role encompassing embryonic development, cellular differentiation, hematopoiesis, lymphopoiesis, inhibition of tumor growth, and general transcriptional repression. Comprising seven subunits, the multi-subunit NuRD complex involves Mi-2 subfamily members CHD3 and CHD4 (Torchy *et al*., 2015).

Both CHD3 and CHD4 exhibit unique remodeling capabilities even in the absence of accessory core subunits, indicating that NuRD complex possess distinct remodeling traits and activities crucial for regulating DNA-dependent processes like repair and transcription. The domain organization of CHD3 and CHD4 includes two conserved plant homeodomain (PHD) fingers, two tandem chromodomains responsible for chromatin organization modification, and a SWI2/SNF-like helicase domain. The PHD domains prevent non-specific DNA binding by the chromodomains while enhancing their affinity towards H3 tails. The ATPase domain strengthens the PHD domains affinity, and vice versa, showcasing an interdependence leading to structural stabilization regardless of ATP presence (Hoffmeister *et al*., 2017; Spruijt *et al*., 2021).

### 3.1.4 Imitation switch (ISWI)

The ISWI family is a crucial player in chromatin remodeling and contains a highly conserved SWI2/SNF2 family ATPase domain that belongs to the superfamily of DEAD/H-helicases, providing the necessary motor for chromatin remodeling. The ATPase unit of ISWI is located in the protein's N-terminal region and includes the DExx and HELICc regions. Conversely, in the C-terminal segment, ISWI contains the HAND-SANT-SLIDE (HSS) domains, crucial for DNA/Histone binding and critical for interaction with the DDT/WHIM domains present in all major heterodimeric ISWI partners. This SLIDE domain interaction, occurring outside the nucleosome, not only enhances ATPase activity but also enables the facilitated movement of DNA along the nucleosome structure (Fig.2) (Grüne *et al*., 2003; Aydin *et al*., 2014).

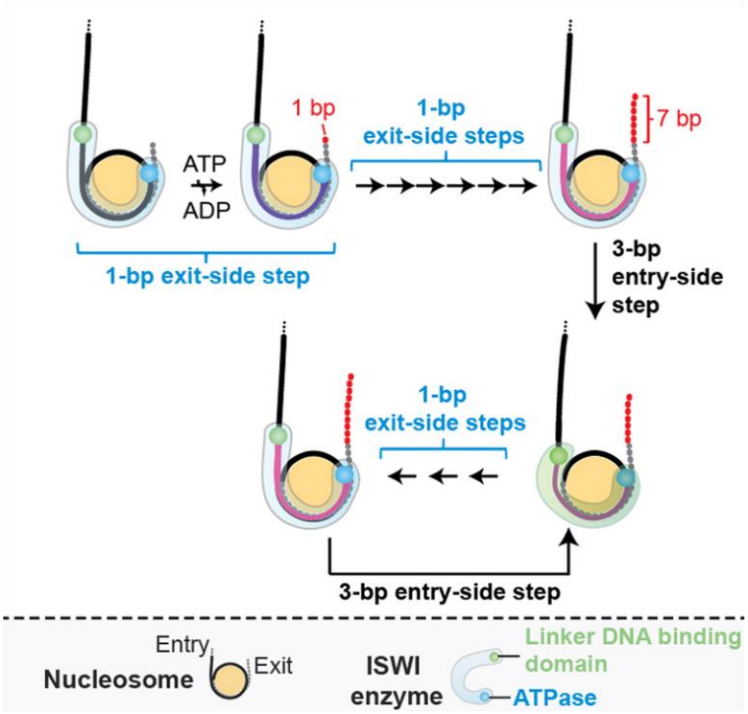


**Fig. 2 | Nucleosome sliding by ISWI.** Nucleosome remodeling involves a 7-bp DNA translocation followed by 3-bp steps towards the exit side. Compound steps consist of 1-bp substeps. Entry-side movement occurs after 7 bp of exit-side translocation, drawing in 3-bp DNA and allowing further base pair movement (adapted from Deindl *et al*., 2013).

The mammalian repertoire of ISWI family of chromatin remodeling ATPase/Helicases consists of two homologues SMARCA5 (SNF2H) and SMARCA (SNF2L), and together with its interacting partners play a vital role in maintenance chromatin structure and function, regulation of gene expression, cell division, DNA-damage repair, gametogenesis and development. The ISWI complexes modify the DNA accessibility of DNA binding and regulatory proteins depending on the interacting partner present, thus enabling the modulation of gene expression across a range of cellular contexts. SMARCA5 has an important role in

early development in mice and other lower organisms, both regulating chromatin structure and contributing to processes involved in cell fate decisions like DNA replication, repair, and transcription via all three classes of RNA polymerase. Dysregulation of SMARCA5 expression has been observed in various cancers such as leukemia, breast, lung and gastric cancer among others (Fig.3) (Corona and Tamkun, 2004; Li *et al*., 2021; Shi *et al*., 2021).

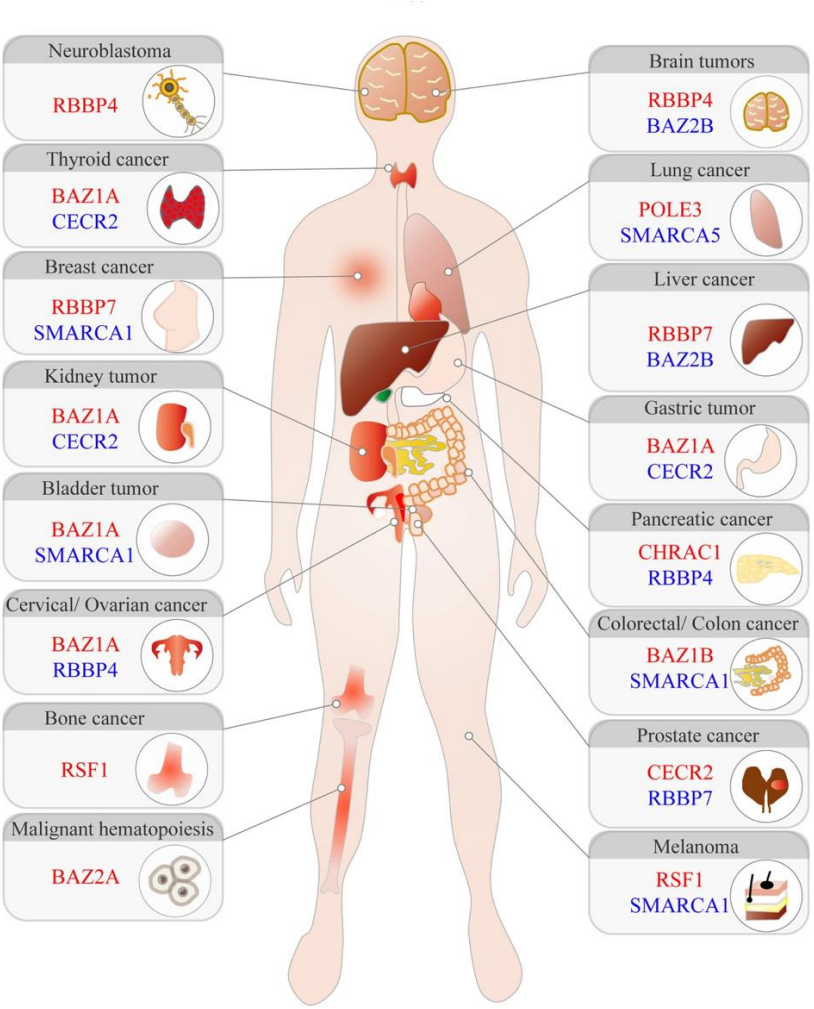


**Fig. 3 | Dysregulation of ISWI family proteins and binding partners in cancer.** The genes that are overexpressed or underexpressed are highlighted in red and blue, respectively (adapted from Li *et al*., 2021).

*Smarca1* and *Smarca5* expression patterns may overlap though they perform distinct functions depending upon developmental context. *Smarca5* deficiency during cerebellum development leads to hypoplasia of the cerebellum and symptoms related to axons. On the other hand, when it is absent in Purkinje neurons after cell division, it contributes to deficiencies in neurochemicals and cognitive changes. *Smarca1* plays a role in regulating cell cycle exits by controlling *Forkhead box G1* (*FoxG1*) levels, which then affects neural function and cortical differentiation. It is worth noting that *Smarca5* levels are higher in actively dividing progenitor cells, while *Smarca1* levels are more prominent in cells that have

completed their differentiation process (Alvarez-Saavedra *et al*., 2014; Goodwin and Picketts, 2018; Picketts *et al*., 2023).

In adult mice, *Smarca1* is expressed notably in the cortex, cerebellum, ovaria, uterus, testes, and placenta. It acts as a widely expressed modulator within the canonical Wnt/β-catenin signaling pathway, a highly conserved relay network where β-catenin plays a central role in transducing Wnt signals to orchestrate cellular responses. Dysfunctions in this pathway are linked to developmental defects and diseases like cancer. Moreover, further analysis has established an association between low *Smarca1* levels and the manifestation of a malignant phenotype (Lazzaro and Picketts, 2001; Eckey *et al*., 2012).

Smarca5 impacts cell cycle dynamics and reduces the expansion of specific *Foxg1*+ neural progenitor. This reduction significantly affects the production of upper layer neurons and impacts the development of callosal neuron projections. The altered expression of clustered protocadherin-β genes and disrupted axon targeting leads to partial agenesis of the corpus callosum. In contrast, Smarca1, modulates *Foxg1* expression, influencing neuronal hypercellularity and brain size without major changes in cortical structure. Smarca1 role in regulating *Foxg1* expression results in the repression of *Foxg1* and the subsequent activation of p21, a cell cycle regulator, facilitating the differentiation of progenitor cells, ultimately controlling brain size. This complex interplay of Smarca1 influences progenitor cell cycles, self-renewal, and neurogenesis timing, enhancing overall cell numbers in the developing neocortex. This suggests that Smarca1 complexes are recruited to the Foxg1 locus to regulate gene expression and promote terminal differentiation (Yip *et al*., 2012; Alvarez-Saavedra *et al*., 2019).

Smarca5 is specifically critical for early embryonic development and adult erythropoiesis, playing a crucial role in regulating gene expression and cell differentiation. During both fetal and postnatal development, *Smarca5* exhibits wide expression and is required for the proliferation and survival of fully committed erythroid progenitors. Additionally, Smarca5 guides the developmental mRNA program of β-selected thymocytes, influencing cell fate decisions in various thymocyte populations. Its inactivation in developing thymocytes activates p53 and apoptosis, impacting the survival of pro-B cells and suppressing hematopoietic development. The absence of *Smarca5* leads to inhibited cell cycle progression at the G2/M phase, causing erythroid defects and severe anemia (Kokavec *et al*., 2017; Zikmund *et al*., 2019, 2020).

Smarca5 also plays a major role in organizing arrays of nucleosomes adjacent to the CTCF binding sites and promotes CTCF binding, contributing to the function of many human gene

regulatory elements. CTCF is a multivalent transcriptional regulator that can impact gene expression directly at promoters or by orchestrating interactions between regulatory elements, and it contributes to the regulation of the three-dimensional structure of chromatin and the formation of chromatin domains. The depletion of *Smarca5* at CTCF sites results in a marked reduction in the surrounding nucleosomal patterns and reduced CTCF occupancy. Smarca5 also plays a part in nucleosome phasing near a variety of transcription factors, driving nucleosomes towards factor binding sites. While Smarca5 is not a universal loading factor for cohesin, it does influence cohesin loading at specific CTCF sites, thereby affecting CTCF-dependent gene expression (Dluhosova *et al*., 2014; Wiechens *et al*., 2016; Barisic *et al*., 2019; Dehingia *et al*., 2022).

The BAZ1B-SMARCA5 protein complex, known as WICH, plays a crucial role near replication fork by orchestrating a network of proteins. This association enables SMARCA5 to target DNA replication sites through its interaction with Proliferating cell nuclear antigen and prevent heterochromatin formation on new DNA strands. BAZ1B also facilitates Topoisomerase I access to replication fork and enhances its function during DNA replication. Moreover, BAZ1B influences replication interference and ISWI nucleosome remodeling activities may enhance the interaction between Topoisomerase II and chromatin, improving functionality. Additionally, BAZ2A regulates H3K27me3 genome occupancy in a TOP2A-dependent manner while interacting with Smarca5 and Topoisomerase IIA. These findings illuminate the complex interplay between chromatin remodeling factors, topoisomerases, and their influence on DNA replication processes (Ribeyre *et al*., 2016; Dalcher *et al*., 2020; Roganowicz *et al*., 2023).

## 3.2 Bromodomain containing proteins

### 3.2.1 Bromodomain

Bromodomain (BRD) is an evolutionarily conserved protein module found in 46 different BRD-containing proteins, primarily recognizing acetylated histones and regulating gene expression through various activities. These proteins can act as scaffolds for larger protein complexes, function as transcription factors and co-regulators, and perform catalytic functions such as methyltransferases, chromatin-remodeling complexes, histone acetyltransferases (HATs) and helicases to engage in chromatin modifications. BRD proteins are expressed in

various issues with broad and variable expression profiles suggesting context-dependent significance (Marmorstein and Zhou, 2014).

The bromodomain presents a unique structural fold characterized by a left-handed four-helix bundle (αZ, αA, αB, and αC) known as the BrD fold. The interhelical αZ-αA and αB-αC loops form a hydrophobic pocket that recognizes the acetylated lysine and other lysine-acylated modifications such as propionyl, succinyl, crotonyl, butyryl, isobutyryl, malonyl or 2-hydroxyisobutyryl with variable affinity. Conserved tyrosine residues found in these loops contribute to this pocket and are present in most bromodomains. Typically, around 110 amino acids in length, bromodomains may play dual roles: first by selecting the substrate, *e.g.*, nucleosomes for acetylation and subsequently promoting stable interactions post-acetylation, leading to an acetylation cascade (Fig.4) (Mujtaba *et al.*, 2007; Nakamura *et al.*, 2007).

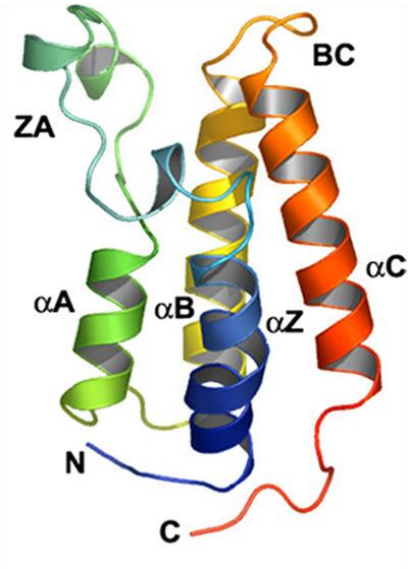


**Fig. 4 | Ribbon Structure of Bromodomain.** The bromodomain showcases a distinctive structure, featuring a specific left-handed four-helix arrangement termed the BrD fold, which includes the αZ, αA, αB, and αC helices. Additionally, it comprises the connecting loops αZ-αA and αB-αC between these helices (adapted from Nakamura *et al.*, 2007).

### 3.2.2 Bromodomain adjacent to PHD zinc finger (BAZ) proteins

BAZ protein complexes usually consist of a heterodimer pairing: an ISWI protein (Smarca1 or Smarca5) and a protein carrying a BAZ domain. These BAZ-containing proteins belong to the BAZ transcription family, including BAZ1A/ACF1, BAZ1B/WSTF, and BAZ2A/TIP5, BAZ2B, that are closely related to other chromatin remodeling proteins RSF1, BPTF and CECR2. Apart from the BAZ domains, these partner proteins also feature AT hooks and/or DDT domains, believed to facilitate in DNA binding (Fig.5) (Marmorstein and Zhou, 2014).

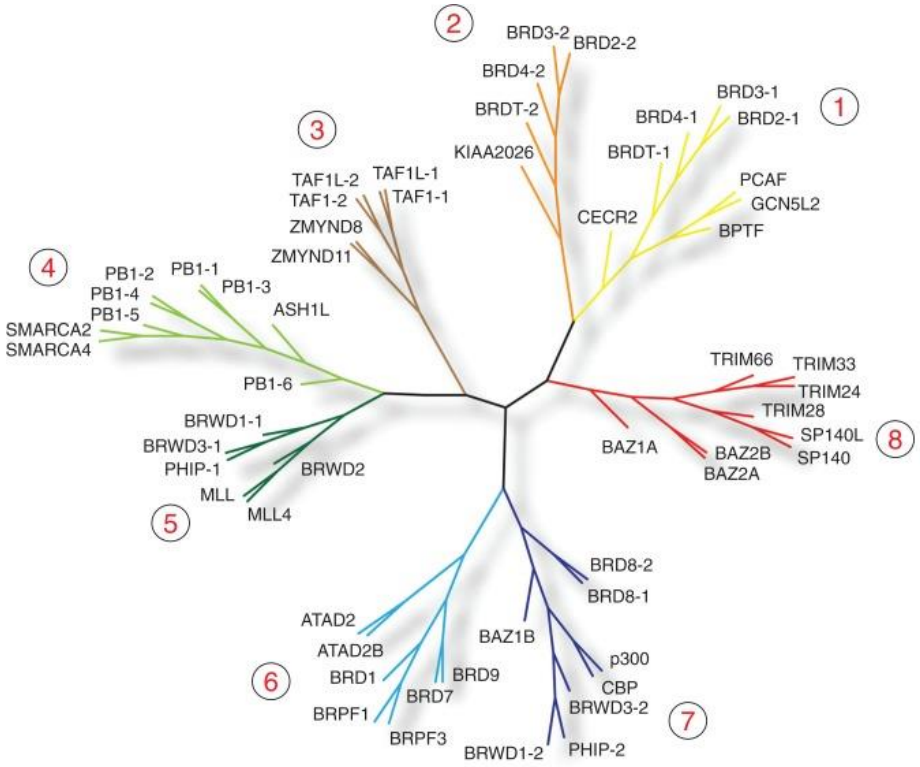


**Fig. 5 | Human bromodomains.** The human bromodomains are classified into eight groups based on their sequence similarity using the neighbor-joining method in MEGA3 software and SMART database, and aligned using Hmmalign with the hidden Markov models of SMART BRDs (adapted from Marmorstein and Zhou, 2014).

BAZ1A, also known as ATP-utilizing chromatin assembly and remodeling factor 1 (ACF1), plays a crucial role as a chromatin remodeler within the ISWI complexes ACF and Chromatin accessibility complex (CHRAC). ACF1 includes distinct motifs like WAC, DDT, WAKZ, PHD finger, and bromodomains, contributing to its diverse functions, such as chromatin assembly, remodeling, and DNA damage repair. Depletion of *Baz1a* influences the expression of genes crucial for nervous system development and function and its recruitment by Histone H3K4 trimethylation emphasizes its involvement in targeted chromatin remodeling of the DNA region. Additionally, BAZ1A plays a role in nucleotide excision repair and accumulates at sites of UV-induced DNA damage based on specific histone acetylation patterns (Fyodorov *et al*., 2004; Zaghlool *et al*., 2016; Koyauchi *et al*., 2022).

The bromodomain adjacent to the zinc finger domain 1B (BAZ1B), also known as Williams syndrome transcription factor (WSTF), operates as a tyrosine kinase crucial in various cellular functions, particularly in chromatin organization mediated by the WSTF ISWI chromatin remodeling complex (WICH) and B-WICH complexes. BAZ1B plays a critical role in DNA damage recovery through the regulation of ISWI factors loading at DNA lesions and support for transcriptional programs vital for survival. Its role as a regulator of neurogenesis supports the suggestion that *Baz1b* haploinsufficiency contributes to neurocognitive

phenotypes in Williams syndrome, as reduced *Baz1b* expression adversely impacts neuronal and neural crest development. Furthermore, mice with *Baz1b* deletion have higher mortality rates when experiencing either heterozygous or homozygous *Baz1b* loss. Silencing *BAZ1B* also effectively suppresses cell proliferation, causing changes in the transcriptome and inhibiting pathways linked to breast cancer cells. This suppression reveals a potential weakness in these cancer cells, identifying BAZ1B as a promising therapeutic target (Lalli *et al*., 2016; Oppikofer, Sagolla, *et al*., 2017; Salvati *et al*., 2022; Pai *et al*., 2024).

Bromodomain adjacent to zinc finger domain protein 2A (BAZ2A), also known as Transcription termination factor I-interacting protein 5 (TIP5), is a crucial component of the nucleolar remodeling complex (NoRC), significantly influencing the transcription of ribosomal RNA. The presence of AT-hooks within BAZ2A is vital for nucleolar targeting, forming a DNA binding motif consisting of a glycine-arginine-proline (G-R-P) tripeptide core flanked by basic amino acids. Recent research has shown variations in AT-hook sequences, with some canonical AT-hooks demonstrating RNA binding capabilities, expanding the known structural and functional diversity of this protein domain. Additionally, BAZ2A/TIP5 contains a PHD recognized for its ability to read methylated H3K4. PHD finger of BAZ2A in complex with unmodified N-terminal histone H3 tail reveals a helical folded-back conformation. This conformation is induced by an acidic patch on the protein surface, which prevents peptide binding in an extended conformation. Notably, elevated levels of *BAZ2A* have been identified in aggressive and recurring prostate cancers, promoting cellular migration. Its overexpression contributes to the regulation of rDNA chromatin organization by modulating DNase I accessibility and binding matrix-associated regions (MARs). *BAZ2A* has been proposed as a potential prognostic marker for aggressive and recurring prostate cancers, positioning it as a promising target for therapeutic intervention (Zillner *et al*., 2013; Filarsky *et al*., 2015; Bortoluzzi *et al*., 2017; Dalle Vedove *et al*., 2022).

Bromodomain adjacent to zinc finger domain protein 2B (BAZ2B), consisting of a bromodomain and a PHD. Specifically, the PHD domain of BAZ2B interacts with unmodified histone H3K4, while the BRD region interacts with acetylated histone marks on H3K14 and H3K16. The binding of the bromodomain to acetylated H3K14, typically linked to gene activation at promoter regions, suggests a potential role for BAZ2B in transcriptional activation. Moreover, studies have highlighted BAZ2B influence over neurodevelopment and hematopoiesis. BAZ2B has been shown to control the reprogramming of human hematopoietic cells, particularly by remodeling chromatin at distal elements of committed progenitors (Bortoluzzi *et al*., 2017; Arumugam *et al*., 2020; Scott *et al*., 2020; Feng *et al*., 2022).

## 3.3 ISWI family chromatin remodeling complexes

Chromatin The ISWI ATPase, SMARCA5, or SMARCA1 is a component of various chromatin remodeling complexes, including NURF, RSF, CECF, WICH, NoRC, CHRAC, and ACF (Dirscherl and Krebs, 2004). The specific functional role of Smarca5 and Smarca1 within each chromatin remodeling complex is determined by their respective binding partners (Fig. 6).

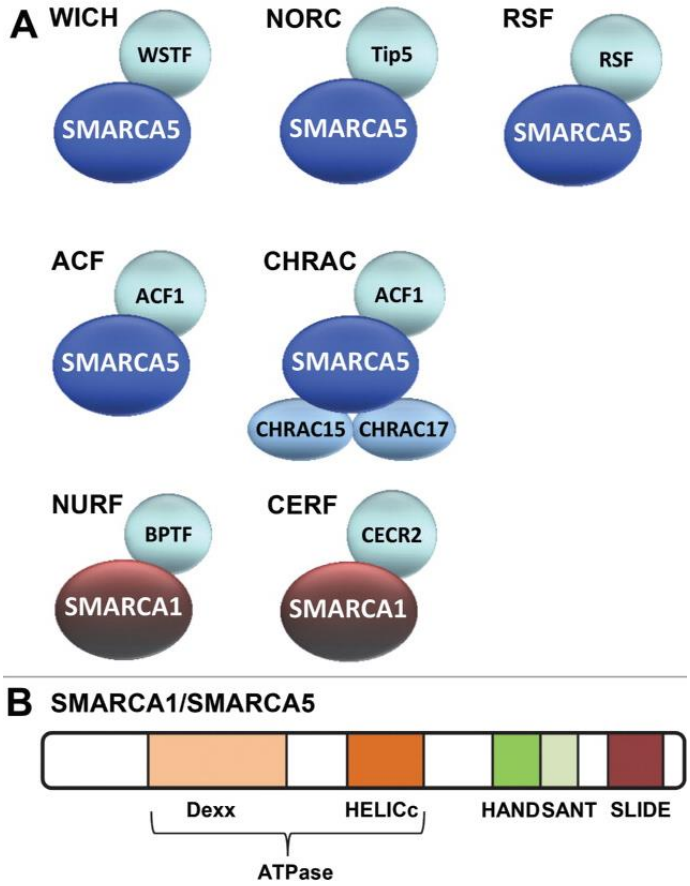


**Fig. 6 | ATP-dependent chromatin remodelers. a**, ISWI family chromatin remodeling complexes: NURF, RSF, CECF, WICH, NoRC, CHRAC, and ACF **b**, Smarca1 and Smarca5 DEAD/H-helicase superfamily locates in its N-terminal region. Its C-terminus contains HAND, SANT, and SLIDE domains (Aydin *et al*., 2014).

### 3.3.1 ATP-utilizing chromatin assembly and remodelling factor (ACF)

The ACF complex is comprised of the SMARCA5 and ACF1, this complex demonstrates nucleosome spacing and contributes to widespread repression across the genome. ACF1 plays a pivotal role in directing ACF to chromatin targets, while Smarca5 drives nucleosome movement, facilitating increased transcription. This positioning of nucleosomes by the ACF complex particularly leads to transcriptional repression at H3K27-methylated regions, implicating it in the characteristic traits of facultative heterochromatin. Additionally, the ACF

complex exhibits ATP-dependent nucleosome remodeling and spacing activities, and supports transcription from chromatin templates and assembles periodic nucleosome arrays alongside core histone chaperones like Nucleosome assembly protein 1 or Chromatin assembly factor 1. It also mediates ATP-dependent chromatin remodeling induced by transcription factors. ACF is capable of bypassing sequence-dependent positioning effects and modulating nucleosome activity through a displacement mechanism influenced by two key features: the N-terminal tail of histone H4 and the length of the extranucleosomal linker DNA. ACF1 preference for binding shifts based on linker DNA length, impacting the catalytic domain of SMARCA5 and affecting nucleosome spacing and sliding (Ito *et al*., 1997; LeRoy *et al*., 2000; Florescu *et al*., 2012; Singh and Ladurner, 2014; Oppikofer, *et al*., 2017a; Wiles *et al*., 2022).

### 3.3.2 Chromatin accessibility complex (CHRAC)

The CHRAC complex, formed by the ACF complex and two histone-fold subunits, CHRAC-14 and CHRAC-16, was initially discovered through its ability to enhance DNA accessibility in in vitro assembled chromatin. This factor played a significant role in improving the regularity of nucleosome fibers, thereby marking the identification of an initial nucleosome spacing factor with both CHRAC and ACF complexes displaying highly similar activities related to nucleosome sliding in vitro. The co-location of CHRAC with ACF1 in developing oocytes and nurse cells suggests CHRAC's involvement in oogenesis. Mild overexpression of both *ACF1* and *CHRAC16* resulted in apoptotic and packaging abnormalities, indicating the crucial role of CHRAC within a specific range during oogenesis. CHRAC proteins form heterodimers and bind directly to DNA and the N-terminus of BAZ1A, amplifying ACF's effectiveness. These complexes are indispensable for spermiogenesis, male fertility, and the maintenance of DNA damage checkpoints and double-strand break repair mechanisms ( Corona, 2000; Börner *et al*., 2016; Scacchetti *et al*., 2018; Laurette *et al*., 2020).

### 3.3.3 Nucleolar remodeling complex (NoRC)

NoRC, a remodeling complex consisting of BAZ2A/TIP5 and Smarca5 recruits DNA methyltransferase and histone-modifying activities to the rDNA promoter, and forms heterochromatin at repetitive genomic regions such as rRNA genes, centromeres, and telomeres formation. NoRC interacts with the rDNA promoter regions of silent genes repressing transcription through chromatin remodeling and the recruitment of Histone Deacetylase 1, DNA Methyltransferase 1, and DNA Methyltransferase 3 Beta. The Transient Abnormal

Myelopoiesis (TAM) domain possesses a unique structure with extended C-terminal extensions that create a surface for binding RNA. Mutations in critical amino acids within this surface disrupt the binding of RNA. The distinct binding specificities of TAM and Methyl-CpG-binding domains (MBDs) to RNA and methylated DNA, respectively, provide insights into NoRC's interaction with non-coding RNA (Anosova *et al*., 2015; Dalcher *et al*., 2020; Chen *et al*., 2021).

BAZ2A, the larger subunit of NoRC, facilitates its recruitment to rDNA through interactions with promoter-bound Transcription termination factor, RNA polymerase I (TTF-I), pRNA, and acetylated H4K16. BAZ2A contains an RNA-binding domain called TAM, which is crucial for silencing rRNA genes. The TAM domain interacts with a long noncoding promoter RNA originating from an alternative rRNA gene promoter. The association of BAZ2A-TAM with this RNA transcript is required for its interaction with the TTF-I which mediates the recruitment of BAZ2A to rRNA genes and subsequent transcriptional repression. BAZ2A domains that recognize posttranslational modifications on histones are essential for recruiting NoRC to chromatin, but the specific mechanism of how these domains recognize site-specific histone tails remains unclear. The acetylation status of BAZ2A, which can be reversed in response to glucose depletion, affects the activity of NoRC, thereby linking rRNA transcription to cellular energy levels (Zhou, 2002; Tallant *et al*., 2015; Feng *et al*., 2022; Roganowicz *et al*., 2023).

### 3.3.4 WSTF–ISWI chromatin remodelling complex (WICH)

WICH plays a role in regulating rRNA transcription by polymerase I and 5S rRNA/7SL RNA transcription by RNAP III and is necessary for transitioning to an active chromatin state in response to environmental stimuli. It comprised of WSTF, Smarca5 and nuclear myosin 1 and is proposed to function as the counterpart of the NoRC complex at the rDNA promoter, promoting active rRNA transcription. B-WICH replaces NuRD to allow the formation of the pre-initiation complex and enables other factors like c-MYC to enhance gene expression by binding to the promoter (Cavellán *et al*., 2006; Barnett and Krebs, 2011).

The B-WICH complex comprises several key subunits, each with distinct functions. Cockayne syndrome protein B (CSB) plays critical roles in transcription-coupled repair and base excision repair. Nuclear RNA helicase II (DDX21) is essential for rRNA transcription and processing. Splicing Factor 3B Subunit 1 plays a crucial role in pre-mRNA splicing, impacting

gene expression. Myb-binding protein 1a is a putative transcription factor that links ribosome biogenesis to Myb-dependent transcription, regulating the cell cycle (Sharif *et al*., 2021).

B-WICH also plays a role in facilitating c-MYC-MAX binding in the intergenic spacer between 5S rRNA genes, leading to histone modifications and transcription. Additionally, c-MYC regulates the expression of RNA pol I factors and influences ribosomal transcription. WSTF knockdown results in the accumulation of the ATPase CHD4, a component of the NuRD complex responsible for establishing a repressive poised state at the promoter (Rolicka *et al*., 2020; Tariq and Östlund Farrants, 2021).

### 3.3.5 Remodelling and spacing factor (RSF)

RSF1 collaborates with SMARCA5, forming the RSF complex. The interplay of RSF1 and SMARCA5 within this complex orchestrates ATP-dependent chromatin remodeling, pivotal for biological processes like transcription regulation, DNA replication, and cell cycle progression. This complex, where RSF1 acts as a histone chaperone, likely contributes to nucleosome assembly. Working alongside the facilitates chromatin transcription (FACT) complex, RSF1 is involved in chromatin remodeling, influencing the positioning of nucleosomes crucial for transcriptional regulation and p53-mediated transcription during apoptosis triggered by DNA strand breaks (Loyola *et al*., 2003; Min *et al*., 2018).

Increased *RSF1* levels have been linked to aggressive tumor behavior and poorer prognosis in various cancers, notably correlating with shorter overall survival and TP53 mutations in breast cancer. In this context, high expression of *RSF1* aligns significantly with p53 expression. Beyond tumor behavior, RSF plays a multifaceted role in nucleosome assembly and chromatin remodeling triggered by diverse growth signals and environmental cues. Recent findings suggest its interaction with centromere protein A histone, hinting at crucial roles during DNA replication and segregation. Interestingly, within the RSF complex, binding to DNA is contingent upon the presence of histones, implying that RSF1 could regulate Smarca5's DNA-binding activity, potentially by obstructing its DNA-binding domain (Sheu *et al*., 2010; Ren *et al*., 2014; He *et al*., 2019).

### 3.3.6 CECR2-containing remodeling factor (CERF)

Cat eye syndrome (CES) is a rare human chromosomal disorder characterized by a highly variable phenotype, including coloboma in the iris and retina, preauricular ear tags and pits, heart defects, kidney defects, skeletal defects, anal anomalies, cleft palate and intellectual

impairment. Among the potential genes associated with CES is Cat eye syndrome chromosome region candidate 2 (CECR2), that forms chromatin remodeling complexes with both SMARCA1 or SMARCA5 (Fig. 7) (Dicipulo *et al*., 2021).

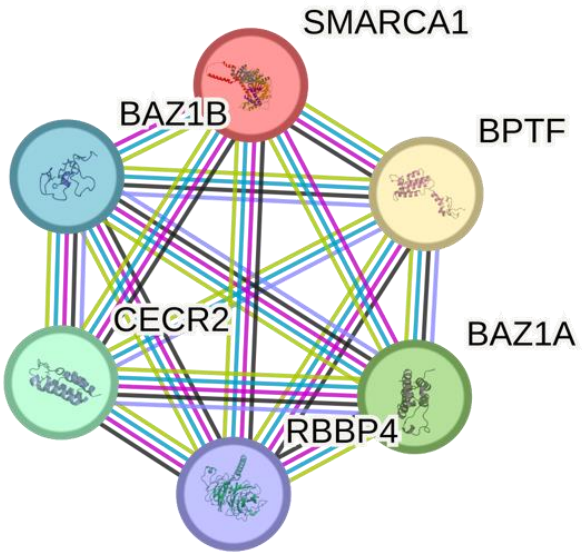


**Fig. 7 | Protein-Protein Interaction Network of CECR2.** The first shell interactors of CECR2 from curated databases are indicated by a blue line, while experimentally determined ones are shown in pink. Confirmed co-expressions are represented by black lines, and protein homology is highlighted with lilac and green lines to suggest interactions predicted by text mining. Created using STRING Database, STRING CONSORTIUM 2023.

The SMARCA1-containing complex CERF functions as a nucleosome-dependent ATPase thereby modifying the accessibility of targeted chromatin regions in both ES cells and testes. This discovery shed light on the role of Cecr2 remodeling protein in spermatogenesis, as evidenced by mutant males displaying reduced litter sizes and lower fertilization rates, possibly due to its impact on *Distal-less homeobox 5 (Dlx5)* modulation. Mutations in *Cecr2* resulted in reduced *Dlx5* expression, with robust *Cecr2* expression in spermatogonia diminishing in spermatocytes and becoming undetectable in spermatozoa. This expression pattern hints at its role in influencing gene expression or chromatin structure in spermatogonia, thereby affecting mature spermatozoa. Loss of *Cecr2* function compromises the fertilizing ability of mature sperm. Female mice with *Cecr2* mutations display varying levels of subfertility, showcasing phenotype variations tied to the severity of the mutation. Severe deficiencies in *Cecr2* may lead to abortions around implantation, whereas milder deficiencies result in embryonal lethality a few days later (Thompson *et al*., 2012; Norton *et al*., 2021).

Cecr2 involvement in neurulation signifies its crucial role in regulating genes responsible for embryonic and post-natal brain development. The *Cecr2* gene exhibits

widespread localization throughout the nervous system, notably in the neural tube, spinal ganglia, forming limbs' mesenchyme, nasal epithelium, eye's lens and neuroretina, and intercostal mesenchyme. Conditional mutations in Cecr2 result in a smaller, wider cochlea, and disorganized stereocilia, indicating its influence on inner ear development, particularly in cases causing exencephaly, which leads to defects in the cochlear ducts' length and orientation of sensory cells in the organ of Corti (Banting *et al*., 2005; Fairbridge *et al*., 2010; Dawe *et al*., 2011; Niri *et al*., 2021).

### 3.3.7 Nucleosome remodelling factor (NURF)

The NURF complex exerts chromatin remodeling activities by targeting specific chromatin regions through interactions with transcription factors and modified histones. NURF consists of Bromodomain PHD finger transcription factor (BPTF), SMARCA1, and pRBAP46/48. This complex orchestrates nucleosome positioning at enhancer elements, essential for regulating transcription initiation, and maintains nucleosome positions downstream of active gene transcription sites. Moreover, NURF's role in remodeling and recruitment at distal insulator sites, crucial for the functional organization of the genome, suggests a functional interplay between distant insulators and active promoters (Alkhatib and Landry, 2011; Ribeiro-Silva *et al*., 2019; Zahid *et al*., 2021).

NURF chromatin remodeling function is pivotal in transitioning stem cells towards a differentiated state. NURF associates with the melanocyte inducing transcription factor (MITF) that regulates the melanocyte lineage in both melanocytes and melanoma cells, co-regulating gene expression, which it is essential for the expression of melanocyte markers and their differentiation into mature adult melanocytes during stimulation at anagen. NURF chromatin remodeling is crucial for transitioning stem cells to a differentiated state. Lacking the NURF subunit *Bptf* in the melanocyte lineage, premature greying occurs due to a lack of mature melanocytes from adult stem cells. Additionally, the increased expression of *BPTF* during tumor progression highlights its potential significance in this context (Koludrovic *et al*., 2015; Laurette *et al*., 2020).

## 3.4 Bromodomain-containing 10 (BRD10)

The evolutionarily conserved BRD10 (previously known as KIAA2026, 9930021J03Rik) gene, classified as a protein coding gene, whose human orthologue is located on short arm of

chromosome 9 (9p24.1), spans a length of 99kbp, and transcribes to an 8kb-long main transcript encoding 2103 amino acids with a calculated molecular mass of 228 kDa. With a total of 6 transcripts or splice variants, BRD10 exhibits a significant level of complexity. This gene has 8 exons, including an unconventional bromodomain encoded within exon 1 and suspected DDT and WHIM domains encoded in exon 3 (Fig.8), the latter making it a prime candidate for a novel ISWI binding partner.

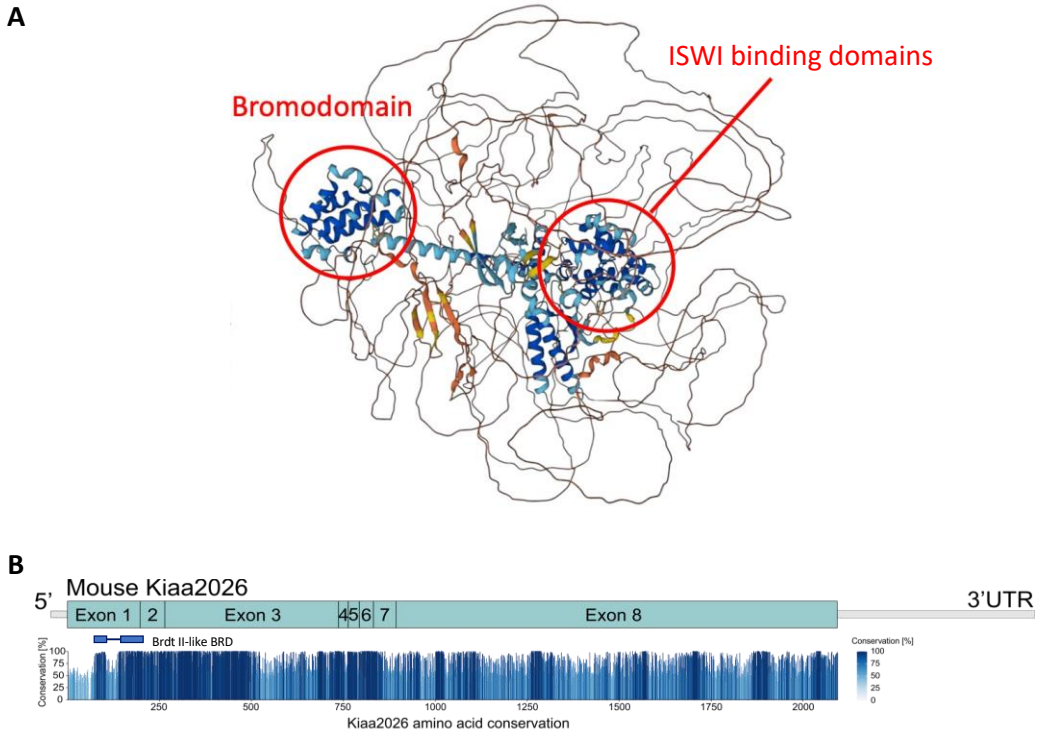


**Fig. 8 | BRD10/KIAA2026. a**, the 3D structure of KIAA2026 with structured regions correspond to bromodomain and ISWI binding domains (DDT + WHIM) was predicted using AlphaFold (Jumper and Hassabis, 2022) **b**, amino acid conservation across amniotes with highlighted highly conserved Brdt II-like bromodomain (created by Dr. Kokavec).

BRD10 was identified by our laboratory in the screen for Smarca5 binding proteins in the mouse model Smarca5$^{+/+}$ Rosa26S$^{FmS5/SFmS5}$ with constitutional expression of N-terminally Strep-FLAG tagged Smarca5 protein in in adult testes and to lower extent also in thymus. Additionally, expression information available at Protein Atlas website revealed BRD10 localization in neuronal and glial cells, along with its presence in germ cells (Fig. 9) and single-cell transcription analysis in mice testes indicated an overlap between the expression profiles of *Smarca5* and *Brd10* in spermatocytes and spermatogonia (Fig. 10).

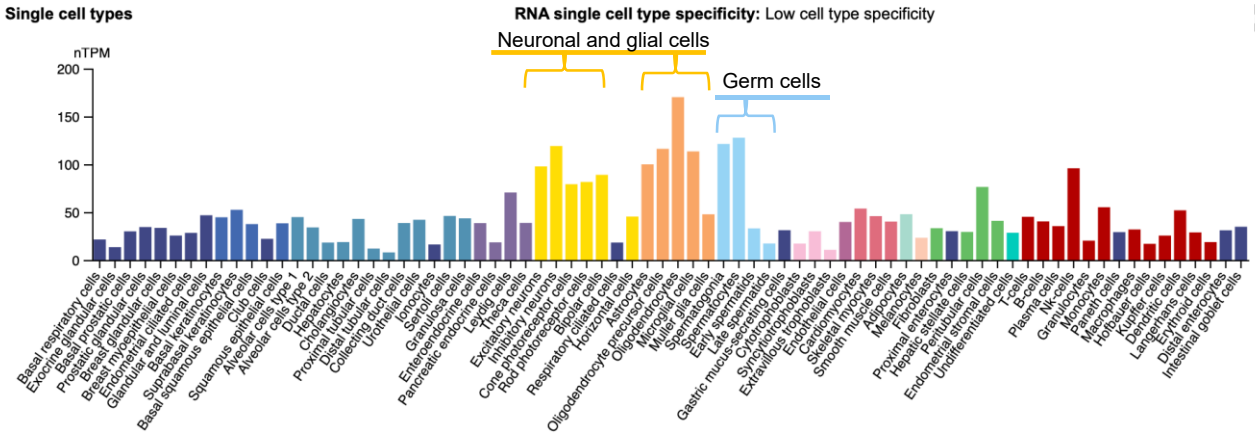


**Fig. 9 | BRD10 expression.** BRD10 by Protein Atlas, revealing its presence in neuronal and glial cells, as well as in germ cells.

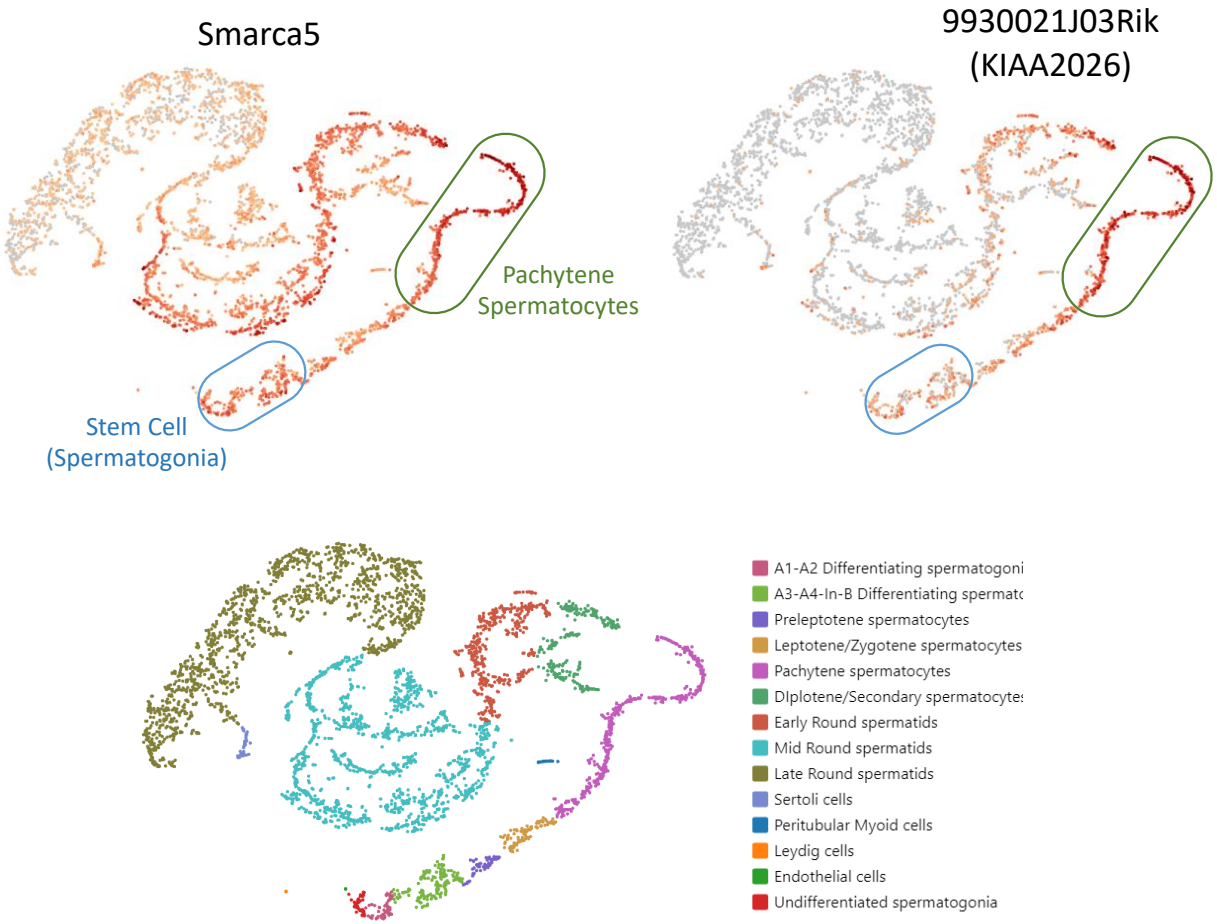


**Fig. 10 | Single cell transcription analysis of mice in testes.** Resemblances were observed in the expression profiles of *Smarca5* and *BRD10* between spermatocytes and spermatogonia **(**created by Dr. Kokavec using https://tanglab.shinyapps.io/Mouse_Male_Germ_Cells/).

# 4 Aims of the Thesis

- Identification of the new interaction partners of SMARCA5
- Exploration of the potential functional networks associated with BRD10/KIAA2026
- Investigation into the role of BRD10/KIAA2026 in the regulation of gene expression

# 5 Material and Methods

## 5.1 Materials

### 5.1.1 Organisms

Subcloning Efficiency DH5α Competent Cells (Invitrogen)

Chemically competent *E. coli* bacteria

Genotype: F- Φ80lacZΔM15 Δ(lacZYA-argF) U169 recA1 endA1 hsdR17(rk-, mk+) phoA supE44 thi-1 gyrA96 relA1 λ-

HEK293 cells

The HEK293 cell line consists of immortalized human embryonic kidney cells were grown in DMEM (with high glucose) supplemented with 10% fetal bovine serum (FBS) and 1% penicillin – streptomycin (PS), maintaining the cells at 37°C with 5% CO2. When reaching 60-80% confluency, the cells were subcultured. Media was discarded, and the cells were washed with PBS to remove any residual media traces.

C57Bl6 Crl

*Mus musculus* standard wild-type inbred model, were housed and maintained at the Czech Centre for Phenogenomics, obtained from Charles River Europe.

### 5.1.2 Tools and Reagents

**Chemicals and buffers**

1 kb Plus DNA Ladder (Invitrogen)

100 bp DNA Ladder (Invitrogen)

150mM NaCl

4x Laemmli protein sample buffer (Bio-Rad)

Agarose powder (Amresco)

Amersham Hybond P 0.45 PVDF blotting membrane (Cytiva)

*Bam*HI (Thermo Scientific)

Buffer E 10x (IBA)

Dithiothreitol (DTT) (Thermo Scientific)

DNA Gel Loading Dye 6X (Thermo Scientific)

DNase Inactivation Reagent (Thermo Scientific)

Ethidium bromide (EtBr)

FastAP Thermosensitive Alkaline Phosphatase (Thermo Scientific)

FastDigest Green Buffer (10X) (Thermo Scientific)

iQ SYBR Green Supermix (Bio-Rad)

Mini Protein Gels NuPAGE 4 to 12%, Bis-Tris, 1.0–1.5 mm (Invitrogen)

Pierce ECL Western Blotting Substrate (Thermo Scientific)

Polyethylenimine stock solution (1mg/ml)

Ponceau S Staining Solution (Thermo Scientific)

Precision Plus Protein Prestained Standards (Bio-Rad)

S.O.C. medium (Invitrogen)

SapphireAmp Fast PCR Master Mix (Takara Bio)

Strep-Tactin Superflow resin (IBA)

SuperSignal ELISA Femto Substrate (Thermo Scientific)

T4 DNA Ligase (Thermo Scientific)

TRIzol Reagent (Thermo Scientific)

WesternBright ECL (Advansta)

*Xho*I (Thermo Scientific)

Dulbecco's Modified Eagle Medium (DMEM)

Inactivated FBS 10%

Penicillin-Streptomycin 1%

DMEM - high glucose (Sigma-Aldrich)

LB (Luria-Bertani) liquid medium

10 g Tryptone

10 g NaCl

5 g Yeast extract

Distilled H2O

Lysis buffer

| | |
|---|---|
| 150 mM NaCl | 1:1000 DTT, 50mM Tris pH 7.5 |
| 0.4% Triton X-100 | 1:1000 TLCK |
| 2 mM CaCl2 | 1:1000 TPCK |
| 2 mM MgCl2 | 1:1000 PMSF |
| 1 mM EDTA | 1:1000 benzonase |
| 1:100 warm up to 95°C $NaVO_4$ | 50mM Tris pH 8.8/2% SDS in H2O - filtered |

PBS (Phosphate Buffered Saline) pH 7.4

1.37 M NaCl

27 mM KCl

100 mM $Na_2HPO_4$

18 mM KH2PO4

Distilled H2O

TBE (Tris-Borate-EDTA) buffer

1M Tris base

1M Boric acid

0.02 M EDTA, pH 8.0

Distilled H2O

TBST (Tris-buffered saline, Tween)

50 mM Tris base

150 mM NaCl

0.1% Tween 20

Distilled H2O

Transfer buffer

25 mM Tris base

192 mM glycine

10% methanol

Distilled H2O

SDS-PAGE Running Buffer

25 mM Tris base

192 mM glycine

0.1% SDS

Distilled H2O

Stripping Buffer

0.1 M Tris-HCl

0.1 M β-Mercaptoethanol

2% SDS

Distilled H2O

**Commercial kits**

DNA-free DNA Removal Kit (Thermo Fisher Science)

Gel/PCR DNA Extraction Fragments Kit (Geneaid)

High-Capacity cDNA Reverse Transcription Kit (Thermo Fisher Science)

High-Speed Plasmid Mini Kit (Geneaid)

Midiprep Plasmid DNA Kit PIF025 (Geneaid)

**Instruments**

Alliance Q9 Chemiluminescence and Fluorescence Imager (Uvitec)

Centrifuge 5415R (Eppendorf)

Centrifuge 5810R (Eppendorf)

Inverted Microscope AE 42 ERGO (Intraco Micro)

LightCycler 480 II (Roche)

Mini Horizontal Agarose Electrophoresis Unit HE33 (Hoefer)

Moticam 1080 Output Microscope Camera (Motic)

NanoDrop Spectrophotometer ND-100 (Thermo Scientific)

Thermal Cycler T100 (Bio-Rad)

UV-transilluminator T2202 (Sigma-Aldrich)

**Software**

ImageJ (NIH)

ImageLab (Bio-Rad)

LightCycler 480 SW (Roche Life Science)

NineAlliance (Uvitec)

R/RStudio

SnapGene (Dotmatics)

### 5.1.3 Oligos and antibodies

**Primers for RT-qPCR**

Table 1: Primers used for RT-qPCR in mouse tissues.

| Primer | Sequence |
|---|---|
| mGapdh(mRNA)-F | ACTTTGTCAAGCTCATTTCCTGGTATG |
| mGapdh(mRNA)-R | TTTCTTACTCCTTGGAGGCCATGTAG |
| mHPRT(mRNA)_F | GCTGGTGAAAAGGACCTCT |
| mHPRT(mRNA)_R | CACAGGACTAGAACACCTGC |
| mKIAA2026(0.2)-F | AAGGAGCAGGAGCTGACCTACG |
| mKIAA2026(0.3)-R | CCTTCGGCCACCTCTTCTTCC |
| mKIAA2026(0.7)-F | CAACAAGGCGTCGGTCAACAC |
| mKIAA2026(0.8)-R | TGCTCTCAGCTGTTCTTCCTGTC |
| Kiaa2026(Rik)-F | GTTCACTAGAGAGCTATGGG |
| Kiaa2026(Rik)-R | ACTTCATATCATCTGAGCCC |
| mSmarca1(mRNA)-F | GGTGTAGCAGTGCTTCTTGGCGTG |
| mSmarca1(mRNA)-R | TCGTTGGAGACAAAGATGTGAGAGCAG |
| mSmarca5(mRNA)-F | AGAATTTGCTTTCAGTTGGAGATTACCG |
| mSmarca5(mRNA)-R | AGATGAGCCAATTCAATCCTCGC |
| FM2_Cecr2 | AACTCTACAAGCTCCTTAGC |
| RM2_Cecr2 | CTCTAGCTTGATGGATTTGATG |

**Antibodies**

Table 2: Primary antibodies used for co-immunoprecipitation and western blot.

| Antigen | Source | Obtained | Cat # |
|---|---|---|---|
| DNA Topoisomerase 2A | Mouse | Novus Biologicals | NBP2-54546 |
| DNA Topoisomerase 2B | Mouse | Novus Biologicals | MAB6348 |
| SNF2h/ISWI | Rabbit | Bethyl | A301-017A |
| FLAG M2 | Mouse | Sigma | F1804 |
| Strep II Tag | Mouse | Novus Biologicals | NBP2-43735 |

Table 3: Secondary antibodies used for co-immunoprecipitation and western blot.

| Antigen | Obtained | Cat # |
|---|---|---|
| Anti-rabbit IgG, HRP-linked | Cell Signaling | 7074S |
| Anti-mouse IgG, HRP-linked | Cell Signaling | 7076S |

## 5.2 Methods

### 5.2.1 Cloning

The transformation of *E. coli* DH5α competent cells was conducted following a specific protocol, with all subsequent steps carried out in chilled tubes on ice. Stocks of 25 µl DH5α cells were initially thawed on ice. After gently mixing the cells with the pipette tip, plasmid preparation was initiated. The plasmid sample was prepared by diluting the expression vector in TE buffer to a concentration of 10 ng/µl. In the transformation process, 10 ng of the plasmid was added to the thawed DH5α cells and gently mixed with the pipette tip. Following this, the mixture was incubated on ice for 30 minutes to allow binding of charged plasmid DNA molecules to bacteria. A heat shock was then performed in a water bath at 42°C for 30 seconds, followed by a 2-minute incubation on ice. To this mixture, 250 µl of room temperature S.O.C. medium (Invitrogen) was added, and the solution was shaken at 225 rpm for 1 hour at 37°C. After the incubation, 500 µl of S.O.C. (Invitrogen) were added to the mixture, and a serial dilution was made at scale 10, 20, 30, 50, 100, 160, and 200 µl. The transformed cells were dropped in the center of a prewarmed LB plate containing 50 µg/ml ampicillin and spread using a hockey stick disinfected with ethanol and flame. The final step involved an overnight incubation of seeded plates at 37°C.

The following day, individual colonies from the LB agar plate were selected and transferred using a sterile pipette tip into 10 ml of liquid LB medium with 50 µg/ml of ampicillin. The culture was loosely covered with sterile aluminum foil that was not airtight. It was then incubated at 225 rpm for 12-16 hours at 37°C. Plasmid DNA was subsequently extracted using the High-Speed Plasmid Mini Kit (Geneaid) or Midiprep Plasmid DNA Kit PIF025 (Geneaid), and its concentration was measured using the NanoDrop Spectrophotometer ND-100 (Thermo Scientific). The obtained plasmids were digested using restriction endonucleases, specifically enzymes *Bam*HI and *Xho*I (Thermo Scientific), for subsequent agarose electrophoresis.

In preparing a standard 1% agarose gel, the agarose powder (Amresco) was mixed with 100 mL 1xTBE in an Erlenmeyer flask. The mixture was then microwaved for 1-3 minutes until complete dissolution of the agarose. Subsequently, the agarose solution was allowed to cool down to approximately 50°C in the water while spinning. Ethidium bromide was added to achieve a final concentration of approximately 0.2-0.5 µg/ml. The agarose was poured into

a gel tray with the well comb in place. The newly poured gel was then either placed at 4°C for 10-15 minutes or left at room temperature for 20-30 minutes until it completely solidified.

For loading samples and running the agarose gel, DNA Loading Dye (Thermo Scientific) was added to each DNA sample (3 µl of Loading Dye per 20 µl of sample). The agarose gel was placed into the gel box (electrophoresis unit) filled with 1xTBE. The gel was run at 60 V for 20 minutes and then at 100 V until the dye line reached approximately 75-80% of the way down the gel. Using a UV-transilluminator, the DNA fragments were visualized. Digested plasmid segments were selected based on their length and extracted from agarose gel using the Gel/PCR DNA Extraction Fragments Kit (Geneaid). Subsequently, their concentration was measured using the NanoDrop Spectrophotometer ND-100 (Thermo Scientific). The dephosphorylation of the cloning DNA vector was carried out using FastAP Thermosensitive Alkaline Phosphatase (Thermo Scientific) to prevent recircularization during ligation. The ligation of fragments was carried out using T4 DNA Ligase in a molecular ratio of 1:3. The incubation was conducted for 12-16 hours at 16°C, followed by heat inactivation for 10 minutes at 65°C. The ligated products were sequenced at the DNA Sequencing Laboratory at the Faculty of Science, Charles University.

### 5.2.2 Transfection

Human Embryonic Kidney (HEK293) cells were seeded at a density of $2.5x10^{\wedge 6}$ cells in a 10 cm dish containing 10 ml of Dulbecco's Modified Eagle Medium (DMEM) supplemented with 10% serum and 1% penicillin-streptomycin. The cells were allowed to grow until reaching 80% confluence, after which they were split one day prior to transfection. The subsequent growth period allowed the cells to reach 50% confluence. For the transfection process, the plasmid mix consisted of 5 µg of plasmid DNA and 250 µl of 150mM NaCl. The PEI mix included 30 µl of polyethylenimine (PEI) per 6 µg of plasmid, along with 250 µl of 150mM NaCl.

Table 4: Transfection Components and Measures.

| Plasmid Mix | PEI mix |
|---|---|
| 5 µg plasmid DNA | 30 µl PEI (6 x µg vector) |
| 250 µl 150mM NaCl | 250 µl 150mM NaCl |

These components were gently mixed by pipetting and left to incubate for 15-20 minutes to facilitate particle formation in the solution. Finally, the plasmid/PEI mixes were delicately dropped onto the surface of the cells in media. For plasmids using a doxycycline-inducible overexpression system, doxycycline was added at a concentration of 1 µg/ml.

### 5.2.3 Fluorescent microscopy

Two days after transfection, cells transfected with plasmids containing GFP were examined for successful transfection using an inverted microscope AE 42 ERGO (Intraco Micro). Subsequently, the captured images were recorded using the Moticam 1080 Output Microscope Camera (Motic).

### 5.2.4 Cell pellet harvesting

To harvest cell pellets, the growth medium was aspirated, leaving approximately 1 ml in the 10 cm culture dish. The cells were then gently scraped from their plate and carefully transferred into a 1.5 ml tube. The next step involved centrifugation at 5000×g for 2.5 minutes at 4°C, resulting in the formation of a cell pellet. Once the centrifugation was complete, the supernatant was aspirated without disturbing the pellet. To cleanse the cell pellet, 1 ml of cold phosphate-buffered saline (PBS) was added, and the tube was vortexed to ensure the proper suspension of cells. A second round of centrifugation at 5000×g for 2.5 minutes at 4°C was performed, and any remaining supernatant was aspirated, leaving the purified cell pellet ready for subsequent analyses.

### 5.2.5 Western blot

In the preceding Western blot procedure, cell pellet was resuspended in Lysis Buffer at a 10x volume. Afterward, it was vortexed and incubated for 30 minutes on ice. Following this, centrifugation at maximum speed for 20 minutes at 4°C was conducted, and the resulting supernatant was transferred into a new Eppendorf tube, constituting the protein lysate. For the input, 1% of the protein lysate was used. 3 µl of 4x Laemmli protein sample buffer (Bio-Rad) were added per 5 µl of the input diluted in Lysis Buffer. Subsequently, the mixture was incubated for 3 minutes at 95°C.

Samples and 3 µl of protein marker Precision Plus Protein Prestained Standards (Bio-Rad), was loaded onto the NuPAGE gel (Invitrogen). The gel ran at 75 V for 15 minutes, then

at 120 V for 1 hour in Running Buffer. The PVDF membrane (Cytiva) was activated with methanol for 1 minute, rinsed with Transfer Buffer, and combined with the gel in a transfer cassette, transferring at 65 V for 1 hour. After transfer membrane was stained with Ponceau S (Thermo Scientific) to facilitate the identification and localization of proteins. Following the staining step, the membrane underwent a thorough wash with water for 2 minutes and three TBST washes for 5 minutes to remove excess Ponceau stain. Following this, the membrane was treated with Stripping Buffer for 15 minutes, then washed with TBST for 5 minutes. It was than blocked with non-fat dry milk for 30 minutes and underwent three 5-minute washes with TBST. Next, the primary antibody (diluted 1:2,000) was applied overnight at 4°C. The membrane was subsequently washed 3 times for 10 minutes each with TBST, followed by application of the secondary antibody (diluted 1:10,000) for 1 hour at room temperature. Following three 5-minute washes with TBST and a subsequent PBS wash, the membrane was dried. It was then stained with a 1:1 mixture of peroxide and luminol. The captured image was analyzed using the Alliance Q9 Chemiluminescence and Fluorescence Imager (Uvitec) along with the NineAlliance (Uvitec) software.

### 5.2.6 Co-immunoprecipitation

The cell pellet was resuspended in Lysis Buffer at a 10x volume. After thorough vortexing, the solution was incubated on ice for 30 minutes and centrifugated at maximum speed for 20 minutes at 4°C. In parallel, Strep-Tactin beads (IBA) were prepared by adding 150 µl of Lysis Buffer to 15 µl of the beads per sample and centrifuging at 300×g for 30 seconds at 4°C. This process was repeated twice. After centrifugation, the remaining Lysis Buffer was discarded to ensure only the beads remained in the pellet. Following that, 15 µl of beads were diluted in 75 µl of Lysis buffer, after which protein lysates were added to the mix. The subsequent step involved incubating the mixture while rotating at 360° for 2 hours at 4°C. The samples were centrifuged at 300×g for 10 minutes at 4°C. Afterward, most of the supernatant was aspirated. Following this, 500 µl of Lysis Buffer was added to the sample, and the mixture was vortexed before undergoing centrifugation at 300×g for 1 minute at 4°C. This washing process was repeated three times. Subsequently, 40 µl of Elution Buffer E (IBA) was added to the sample, which was then incubated for 10 minutes at room temperature. The beads were then sedimented by centrifugation for 10 minutes at 4°C at 500×g, and the resulting supernatant was transferred to a new tube.

5 µl of 4x Laemmli protein sample buffer (Bio-Rad) were added per 20 µl of the sample. The mixture was then incubated for 3 minutes at 95°C. Subsequently, up to 20 µl of the sample and 3 µl of protein marker Precision Plus Protein Prestained Standards (Bio-Rad) were loaded onto the NuPAGE gel (Invitrogen). The gel was run at 75 V for 15 minutes followed by 120 V for 1 hour in Running Buffer. Afterward, PVDF membrane (Cytiva) was activated with methanol for 1 minute and rinsed with Transfer Buffer. The NuPAGE gel and the membrane were assembled in the transfer cassette and subjected to transfer at 65 V for 1 hour. Membrane was washed with TBST for 5 minutes, followed by a 15-minute wash with Stripping Buffer, and another TBST wash for 5 minutes. Next, it was blocked with non-fat dry milk for 30 minutes and washed 3 times with TBST for 5 minutes. Finally, primary antibody, diluted at a ratio of 1:2,000, was applied overnight at 4°C on a rocker.

Following the primary antibody incubation, membrane was washed 3 times with TBST for 10 minutes and secondary antibody, diluted at a ratio of 1:10,000, was applied and incubated for 1 hour at room temperature on the rocker. This was followed by another round of 3 washes with TBST for 5 minutes each, followed by a PBS wash. The membrane was then dried, and it was stained with a mixture of peroxide and luminol (1:1) from either the WesternBright ECL (Advansta) or SuperSignal ELISA Femto Substrate (Thermo Scientific) Western blotting detection kits. Finally, the image was captured by Alliance Q9 Chemiluminescence and Fluorescence Imager (Uvitec) and analyzed by NineAlliance (Uvitec) software.

### 5.2.7 Samples preparation for mass spectrometry

For each cell pellet, a Lysis Buffer 10x the volume of the pellet was added, comprising 150 mM NaCl, 50mM Tris pH 7.5, 0.4% Triton X-100, 2 mM CaCl2, 2 mM MgCl2, 1mM EDTA and proteinase inhibitors 1:1000 of TurboNuclease, 1:1000 TLCK, TPCK, PMSF, and 1:100 NaVO4 (pre-warmed to 95°C), with the exclusion of DTT. The solution than underwent a 30-minute incubation on ice, following which the volume was increased to 10 ml and further incubated for 10 minutes on ice. After centrifugation at maximum speed for 10 minutes at 4°C, 30 µl of 50% Strep-Tactin beads solution were added per each sample. Subsequently, they were washed three times with 1 ml of Lysis buffer and sedimented through centrifugation for 1 min at 200×g at 4°C. Subsequently, an equal number of beads was added to each protein lysate and incubated for 3 hours rotating at 360° at 4°C. Further centrifugation at 500×g for 1 minute at 4°C and Lysis buffer wash removed all non-precipitated proteins. Subsequently, beads were washed twice with 800 µl of 150 mM NaCl was added to neutralize the detergents. 100 µl of

Elution buffer was added to the sample, which was then incubated for 20 minutes on ice. The beads were sedimented through centrifugation at 500×g for 1 minute at 4°C, and the resulting supernatant was transferred to the new Eppendorf tube. The precipitated proteins obtained from this process were subsequently sent to the Proteomics facility at BIOCEV for mass spectrometry analysis.

### 5.2.8 RNA isolation

For RNA isolation intended for qPCR analysis, the cells from the cerebrum, cerebellum, liver, and gonads underwent a series of steps. Initially, mice were euthanized by either cervical dislocation or $CO_2$ inhalation, and their organs were promptly dissected and transferred to tubes on ice. Subsequently, the dissected tissues were washed and resuspended in 1 ml of PBS, followed by centrifugation at 300×g for 1 minute at 4°C. Subsequently, the tissues were resuspended in 500 µl of Trizol Reagent (Invitrogen), and the samples were stored at -80°C for subsequent processing.

For Trizol RNA isolation, samples had to be incubated for 5 minutes at room temperature. Following this, 100 µl of chloroform was added, and the samples were vortexed, followed by an additional incubation period of 3 minutes at room temperature. Subsequently, the mixture underwent centrifugation for 15 minutes at 12,000×g and 4°C. After centrifugation, the upper aqueous phase was carefully pipetted into a tube containing 500 µl of chloroform. The samples were vortexed and again centrifuged for 15 minutes at 12,000×g and 4°C. The upper aqueous phase was then transferred into a tube with 500 µl of 100% isopropanol and 10 µg of glycogen. After thorough mixing, the sample was incubated for 10 minutes at room temperature. Then a centrifugation step for 10 minutes at 12,000×g at 4°C followed. The resulting pellet was washed in 1 ml of 75% ethanol and then resuspended in RNase-free water.

After isolating the RNA, it underwent centrifugation for 5 minutes at 10,000×g at 4°C, and then the supernatant was discarded. Subsequently, the sample was left to air-dry at room temperature. To eliminate contaminating DNA from the RNA samples, the DNA-free DNA Removal Kit (Thermo Fisher Science) protocol was employed, followed by inactivation through incubation for 3 minutes at room temperature with DNase Inactivation Reagent (Thermo Fisher Science). Following this, the sample underwent centrifugation for 2 minutes at 10,000×g at 4°C, and the supernatant was pipetted into a new tube.

### 5.2.9 Reverse transcription and Quantitative PCR

A total of 2 µg of RNA from the previous step was used in the reverse transcription process using the High-Capacity cDNA Reverse Transcription Kit by Thermo Fisher Science, including MultiScribe Reverse Transcriptase. The obtained cDNA was diluted to a concentration of 20 µg/ml and subsequently used for qPCR reactions using the iQ SYBR Green Supermix, consisting of SYBR Green I dye, a specialized buffer, hot-start iTaq DNA Polymerase, and qPCR-qualified dNTPs in the LightCycler 480 II. All samples were run in triplicates.

Table 5: qPCR Protocol Parameters.

| | | |
|---|---|---|
| 50 °C | 2 min | |
| 95 °C | 10 min | |
| 95 °C | 15 s | 45x |
| 60 °C | 1 min | |
| 72 °C | 10 s | |
| 95 °C | 5 s | |
| 65 °C | 1 min | |
| 97 °C | 0,11 °C/s | |
| 37 °C | 2,5 °C/s | |

| | |
|---|---|
| iQ SYBR Green Supermix | 4 µl |
| Nuclease free H2O | 3.35 µl |
| Primer mix: Forward and Reverse (10 µM) | 0.4 µl |
| DNA 2 µg | 0.25 µl |
| Total | 8 µl |

# 6 Results

## 6.1 Expression Plasmids Preparation

In this thesis, creating expression plasmids are essential for successful overexpression in HEK293 cells and subsequent co-immunoprecipitation assays. To construct expression plasmids for transient expression, the pcDNA3.1 backbone was used and modified to include 2xFLAG and StrepTagII. The pcDNA3.1 vector is a versatile platform that contains the necessary components for easy use and high-level expression. It comprises the cytomegalovirus (CMV) enhancer-promoter, multiple cloning sites including *Bam*HI and *Xho*I restriction sites, the Bovine Growth Hormone (BGH) polyadenylation signal, and a transcription termination sequence to ensure mRNA stability. Additionally, it features the SV40 origin for episomal replication to aid in vector rescue in cell lines expressing the large T antigen, as well as an Ampicillin resistance gene and pUC origin for efficient selection and maintenance in *E. coli*.

The addition of 2xFLAG and StrepTagII in pcDNA3.1 is essential for subsequent protein analysis and purification. The Flag-tag enables detection using anti-Flag antibodies, allowing various analyses including protein purification, co-immunoprecipitation, and Western blotting. Its sequence motif NH2-DYKDDDDK-COOH significantly improves antibody affinity for tandem purification. StrepTagII, an eight-residue minimal peptide sequence (Trp-Ser-His-Pro-Gln-Phe-Glu-Lys), with intrinsic affinity toward Strep-Tactin ensures specific purification with minimal non-specific interactions due to its small size which doesn't interfere with protein folding or require post-purification tag removal. Additionally, it efficiently attaches to supports without leaching providing a robust resin ideal for reliable recovery and reuse in purifications.

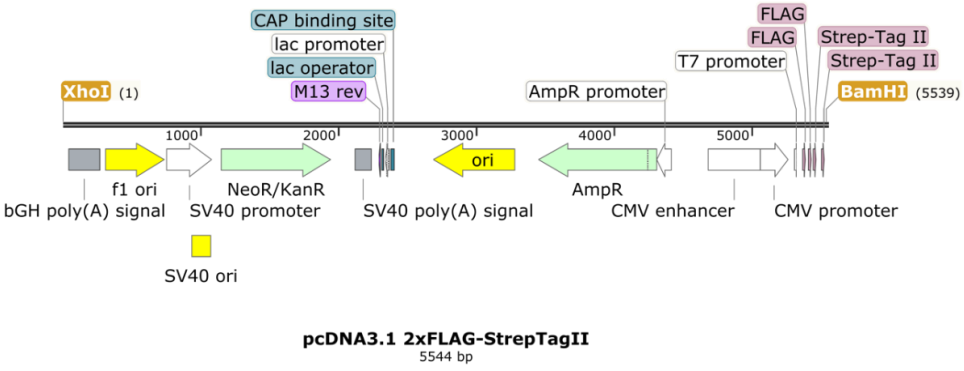


**Fig. 11 | pcDNA3.1 2xFLAG-StrepTagII.** 5544 bp long backbone with *BamH*I and *Xho*I restriction sites, highlighted gene for ampicillin resistance and FLAG-Strep-Tag II in the proximity of *BamH*I restriction site. Created with SnapGene.

The plasmid containing the mouse cDNA of *Kiaa2026/Brd10* gene in pUC-GW-Amp vector with HA and V5 tags was synthesized by AZENTA (Germany). It was then transfected and multiplied in DH5α cells. The isolated plasmid from cell culture underwent digestion by *Bam*HI and *Xho*I enzymes to cut out the Kiaa2026 cDNA sequence, which was later extracted from agarose gel. Similarly, pcDNA3.1 backbone with N-terminal Strep-FLAG Tag underwent digestion by BamHI and XhoI enzymes before being extracted from agarose gel.

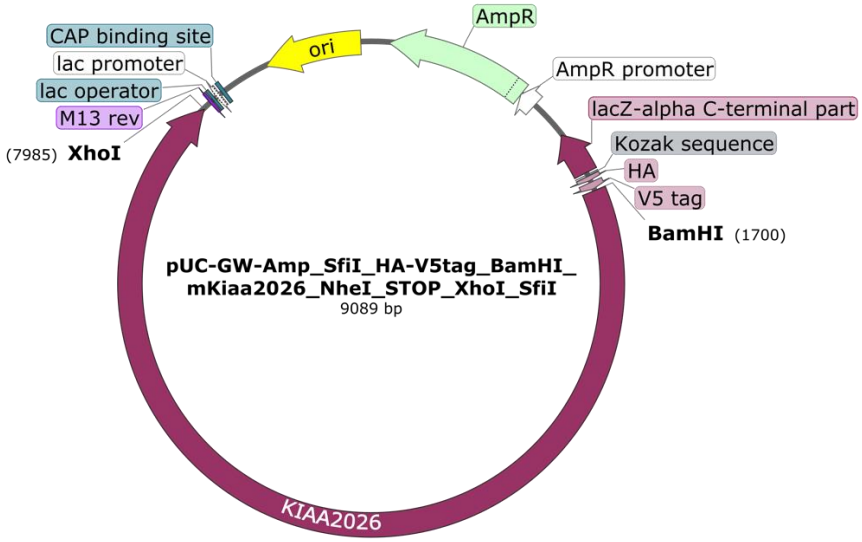


**Fig. 12 | pUC-GW-Amp mKIAA2026.** 6282 bp long mKIAA20226 in 9089 bp long pUC-GW-Amp vector plasmid with *BamH*I and *Xho*I restriction sites. Created with SnapGene.

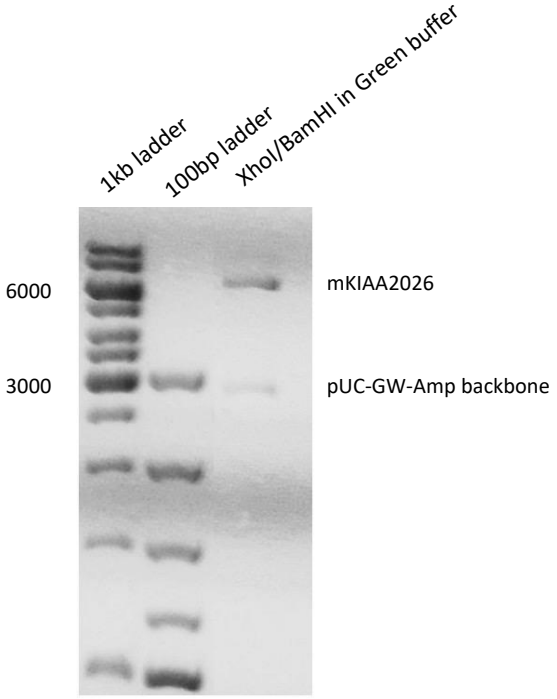


**Fig. 13 | pUC-GW-Amp mKIAA2026 double digested with *BamH*I and *Xho*I in Green buffer.** Gel shows two bands, approximately 6000 and 3000 bp long. mKIAA2026 with expected length of 6285 bp was isolated from gel for further cloning.

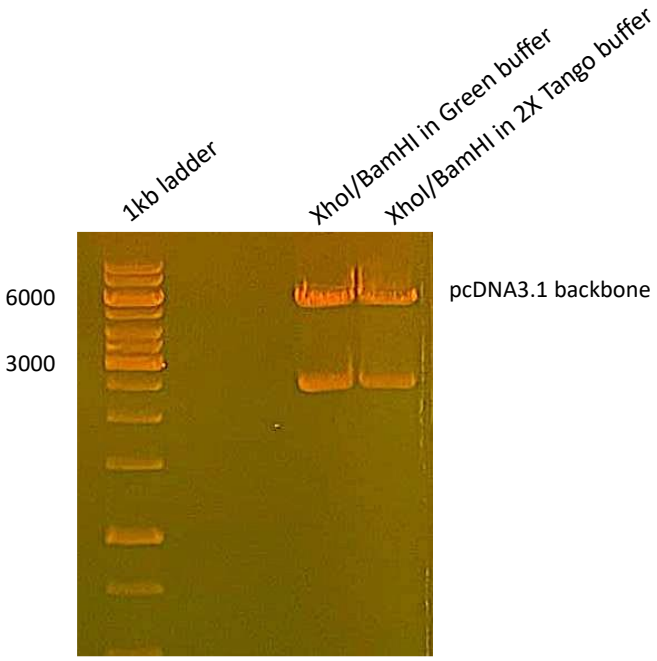


**Fig. 14 | pcDNA3.1. double digested with BamHI and XhoI in Green and 2xTango buffers.** pcDNA3.1 backbone 5538 bp long was isolated from gel.

Non-compatible ends after digestion, potentially minimizing the chances of vector re-ligation, but to guarantee proper ligation, the vector pcDNA3.1 was phosphorylated using FastAP Thermosensitive Alkaline Phosphatase before performing the ligation. The resulting ligation product was then transfected into DH5α cells and colonies were subsequently screened by PCR to validate successful transfection.

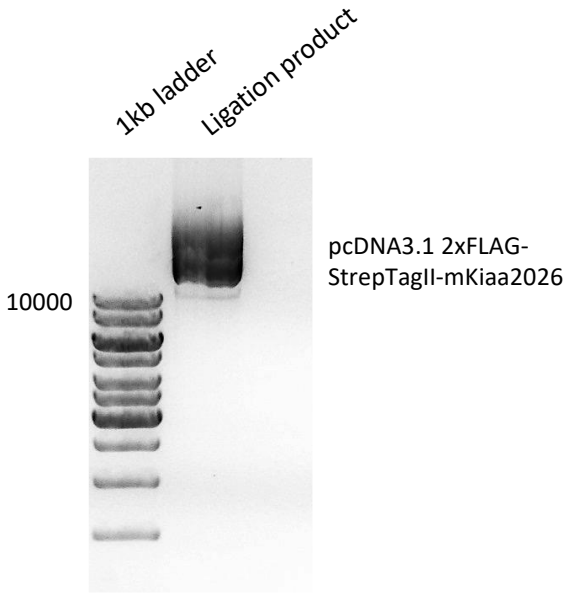


**Fig. 15 | pcDNA3.1 2xFLAG-StrepTagII_BamHI-mKiaa2026XhoI-2.** The size of ligation product was verified before further transfection. This band shows more than 10kb length, suggestion successful ligation.

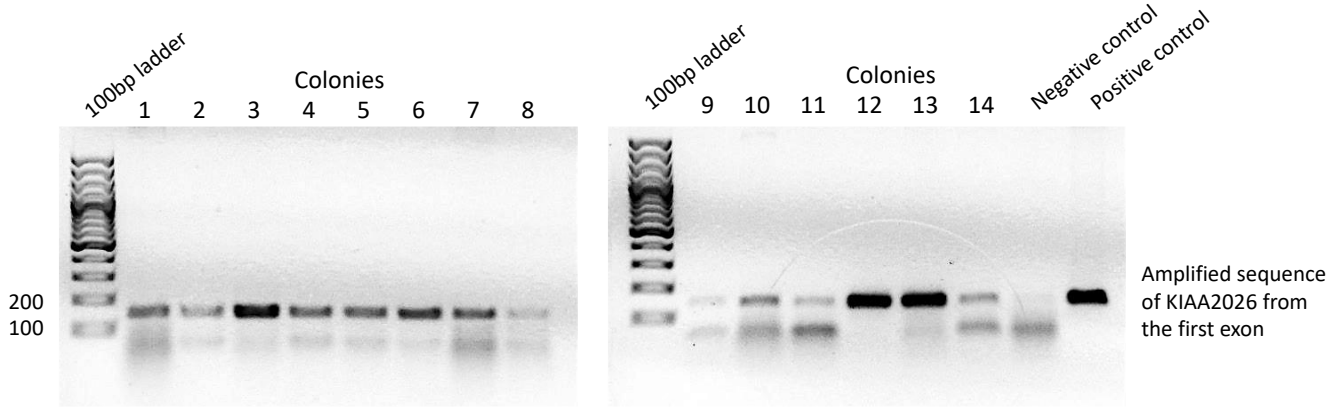


**Fig. 16 | Bacterial colony PCR screening to validate successful transfection.** A 143bp amplification product was obtained using primers mKIAA2026(0.2)-F and mKIAA2026(0.3)-R, with the pUC-GW-Amp-mKIAA2026 plasmid serving as the positive control.

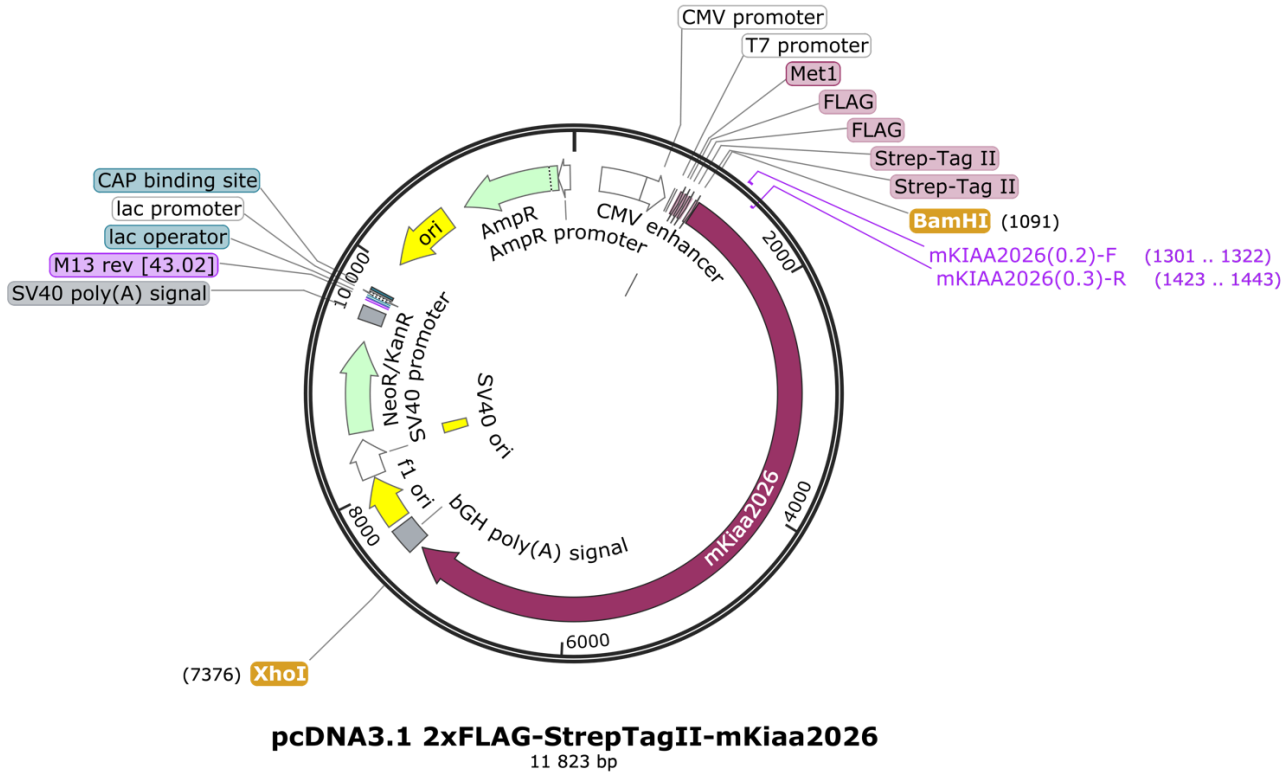


**Fig. 17 | pcDNA3.1 2xFLAG-StrepTagII-mKiaa2026.** Ligation product containing pcDNA3.1 2xFLAG-StrepTagII vector and mKiaa2026 insert with primers for PCR screening and *BamHI*/*Xho*I restriction sites. Created with SnapGene.

Subsequent restriction digestion (Fig. 18) and sequencing (Fig. 19) revealed unexpected patterns and a lack of the desired sequences in the plasmid.

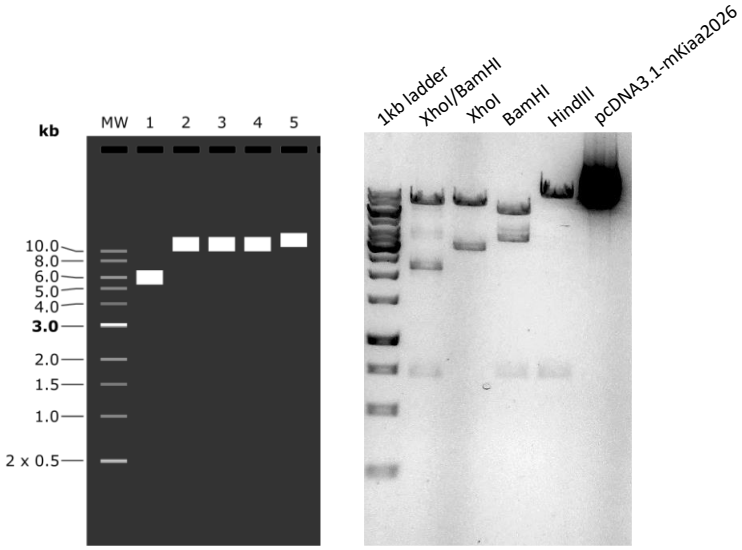


**Fig. 18 | pcDNA3.1 2xFLAG-StrepTagII-mKiaa2026 digested with *BamH*I, *Xho*I, *HindIII* and double digested with *XhoI/BamH*I.** Scheme on the left represents expected digestion pattern (created with SnapGene).

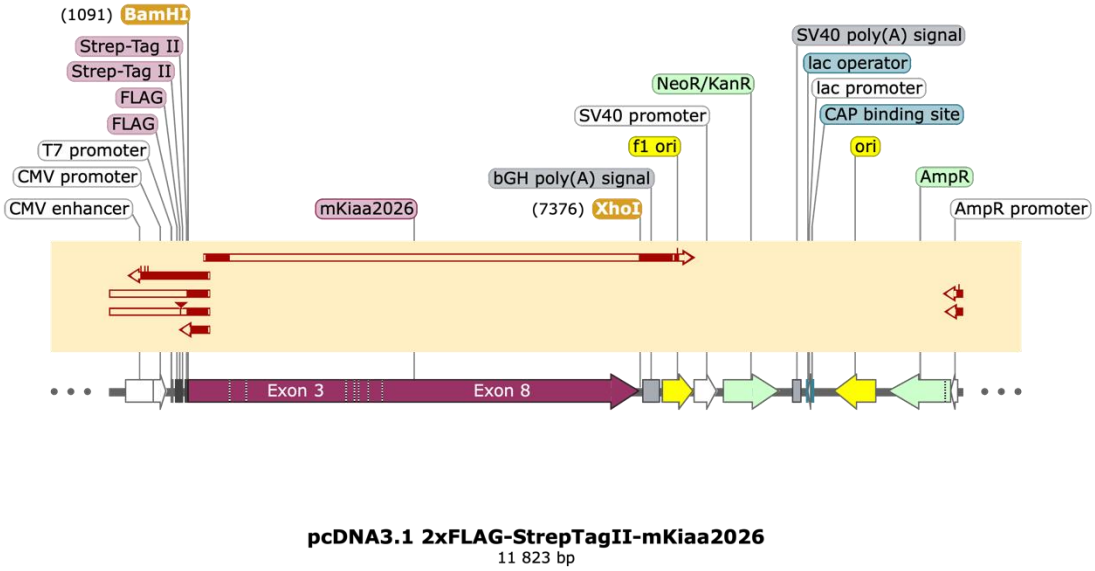


**Fig. 19 | Sequencing alignment with pcDNA3.1 2xFLAG-StrepTagII-mKiaa2026.** Created with SnapGene.

These findings led to the conclusion that the construct might be too large for the cloning process. As a result, Dr. Kokavec utilized NEB PCR Cloning, encompassing PCR, ligation, and bacteria transfection, to create a transgenic strain with a conditional deletion, while my involvement was limited to follow-up sequencing. Subsequent deletion plasmids were then generated, as demonstrated in the following table.

Table 6: Plasmids with conditional deletion.

| Plasmid Name | Deletion Range (AA) | Structural Alterations and Residual Domains |
|---|---|---|
| pcDNA3.1-FlagStrepTag-mKIAA2026 $^{1-195}$ | Δ199-2094 | Only Bromodomain |
| pcDNA3.1-FlagStrepTag-mKIAA2026 $^{1-757}$ | Δ758-2094 | Minimal protein |
| pcDNA3.1-FlagStrepTag-mKIAA2026 $^{1-895}$ | Δ896-2094 | Minimal protein + IBM-C |
| pcDNA3.1-FlagStrepTag-mKIAA2026 $^{195-757}$ | Δ1-194<br>Δ758-2094 | ISWI binding module |
| pcDNA3.1-FlagStrepTag-mKIAA2026 $^{196-895}$ | Δ1-195<br>Δ896-2094 | ISWI binding module + IBM-C |

The plasmids contain either bromodomain or ISWI binding module, or both. Bromodomain recognizes acetylated histones, while the ISWI binding module consists of DTT domain for binding to SLIDE domain of ISWI proteins, WHIM1 and WHIM2 domains for interacting with nucleosomal linker DNA, and presumptive nuclear localization signals NLS1 and NLS2 required for targeting to nucleus. Additionally, IMB-C is a highly conserved region in the C terminus of the ISWI binding module. Plasmids were than used for further western blot and co-immunoprecipitation to distinguish specific domains of KIAA2026 that interact with Smarca5 and other proteins. The scheme below illustrates each plasmid where green represents the N-terminal bromodomain, blue represents the DDT domain, orange indicates the WHIM1 and WHIM2 domains, and yellow shows the IMB-C domain (Fig. 20).

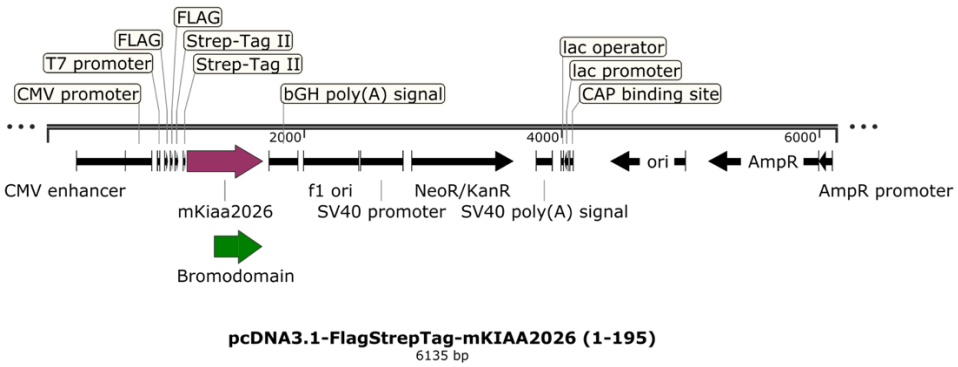

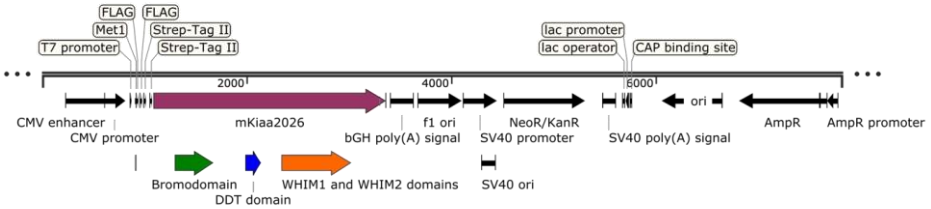


**pcDNA3.1-FlagStrepTag-mKIAA2026 (1-757)**
7812 bp

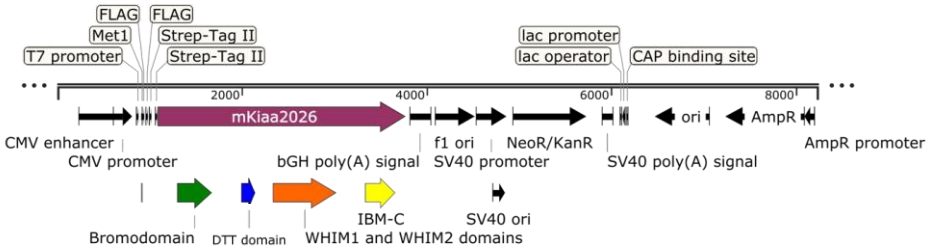


**pcDNA3.1-FlagStrepTag-mKIAA2026 (1-895)**
8229 bp

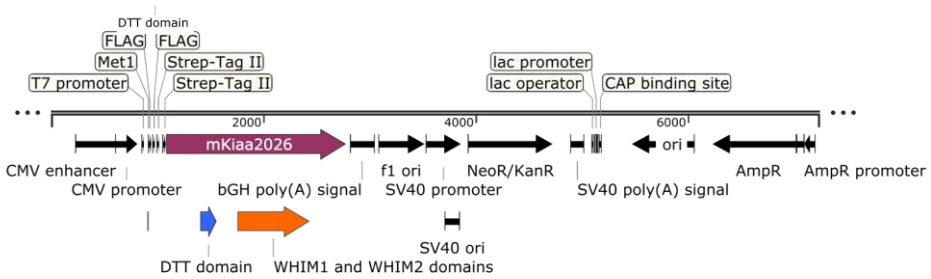


**pcDNA3.1-FlagStrepTag-mKIAA2026 (195-757)**
7227 bp

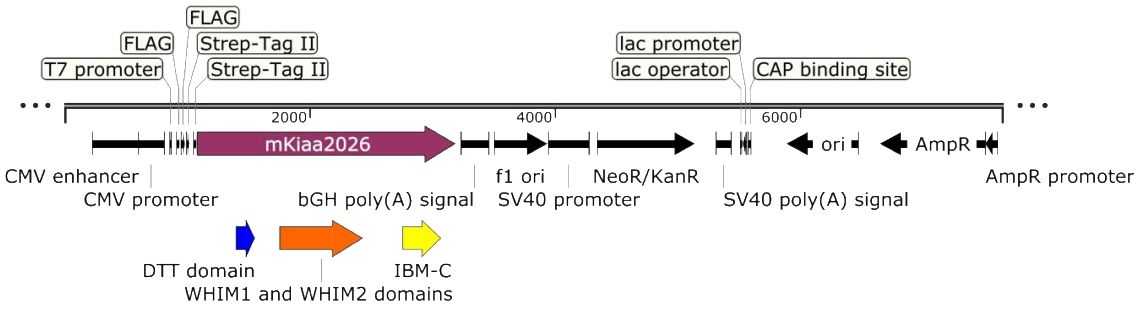


**pcDNA3.1-FlagStrepTag-mKIAA2026 (196-895)**
7644 bp

**Fig. 20 | Schematic Representation of Plasmids Containing Bromodomain and ISWI Binding Module.**

## 6.2 Tissue-specific KIAA2026 expression

Based on Protein Atlas data, KIAA2026 expression is tissue-specific. RT-qPCR was performed on samples from different stages and organs of mice to analyze the expression of Smarca5, Smarca1, CECR2, and various exons of KIAA2026. The primary goal was to identify any potential similarities in their expression patterns or co-expressions across different stages and tissues. RNA was isolated from embryonic stage of E14.5 brain, liver, testes and ovaries; postnatal days 2 brain, cerebellum and testes; as well as postnatal day 9 brain, cerebellum and testes. Absolute quantification has been performed to analyze gene expression and calculate the amount of DNA molecules. ANOVA was used to assess significant differences in log expression levels across various developmental stages.

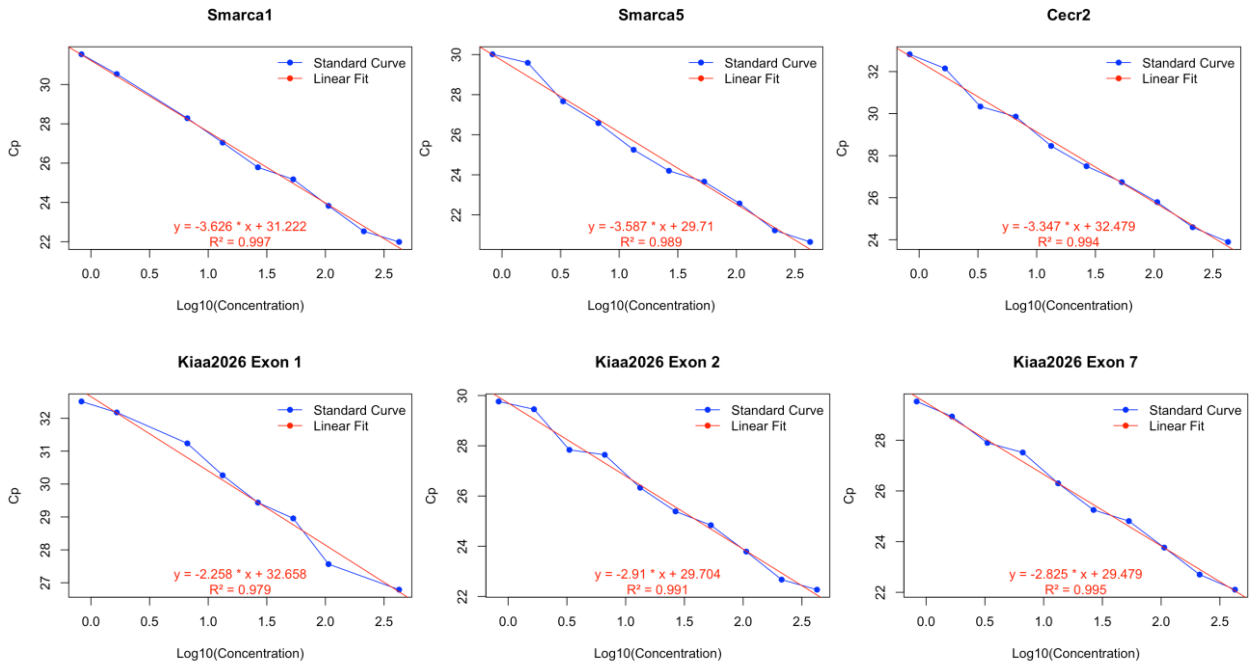


**Fig. 21 | Standard curves for each pair of primers.** Each graph includes regression equations, along with their corresponding coefficient of determination ($R^2$), illustrating the relationship between the crossing point (Cp) values obtained from qPCR and the initial amount of template DNA in ng.

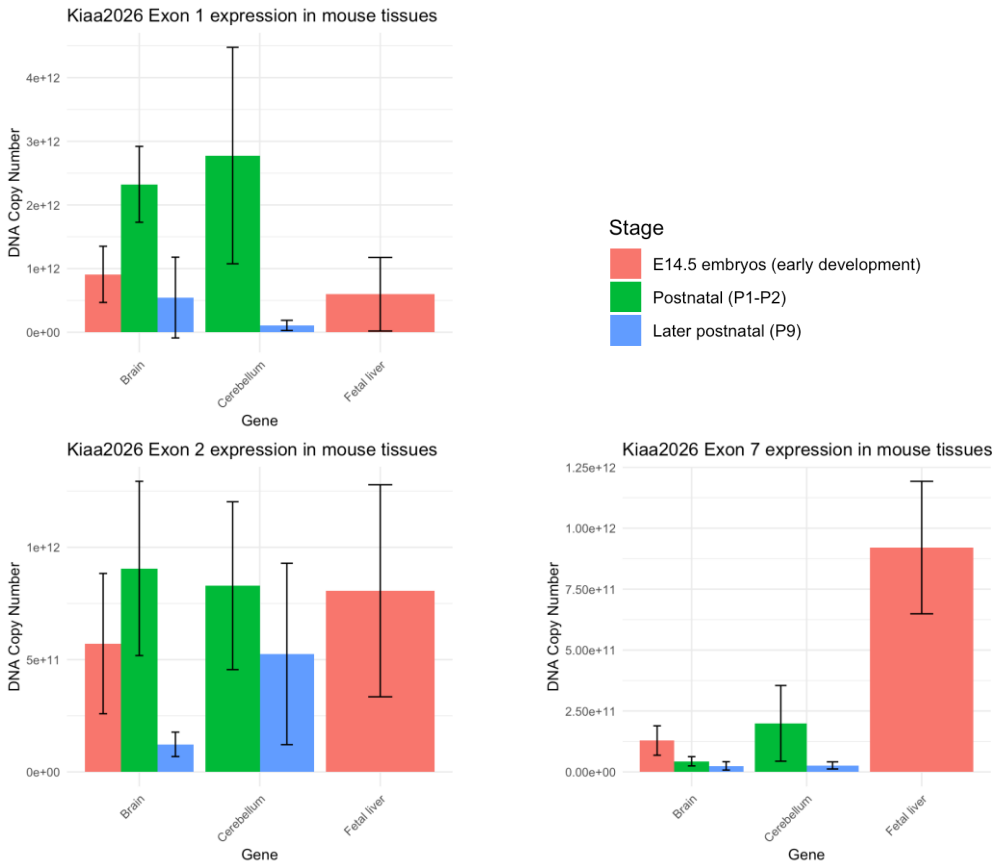


**Fig. 22 | Gene expression profiles of KIAA2026 exons across brain, cerebellum, and fetal liver at different developmental stages.** Embryonal stages were depicted in pink, postnatal days 1-2 were represented by green, and postnatal day 9 was shown in blue.

A consistent decline in expression levels is observed in the brain for exons 1 and 2 of Kiaa2026, from postnatal day 2 (P2) to the embryonic stage (E14.5), and then to postnatal day 9 (P9). In contrast, exon 7 exhibits a declining trend in expression levels from E14.5 to P2 to P9. Specifically, despite the lack of statistical significance in individual exon analyses, a pattern emerges indicating a potential decline in expression levels as brain development progresses from the embryonic stage to postnatal stages. This observed decreasing trend consistently across multiple exons of Kiaa2026 suggests a possible overall regulatory mechanism or developmental pattern associated with the expression of this gene during brain development from embryonic to early postnatal stages.

For Exons 1 and 2 of Kiaa2026 in the cerebellum, a consistent decreasing trend is observed in log expression levels from postnatal day 2 (P2) to postnatal day 9 (P9). This decreasing trend suggests a potential developmental regulation or alteration in the expression patterns of these exons as the cerebellum progresses from an earlier to a later postnatal stage. However, in contrast to Exons 1 and 2, Exon 7 of Kiaa2026 in the

cerebellum does not exhibit statistically significant differences between these stages. The absence of significant differences suggests relative stability or consistency in the expression levels of Exon 7 from P2 to P9 in the cerebellum. Additionally, across all three exons of Kiaa2026 studied, a consistent pattern emerges in the fetal liver, indicating consistently lower log expression levels.

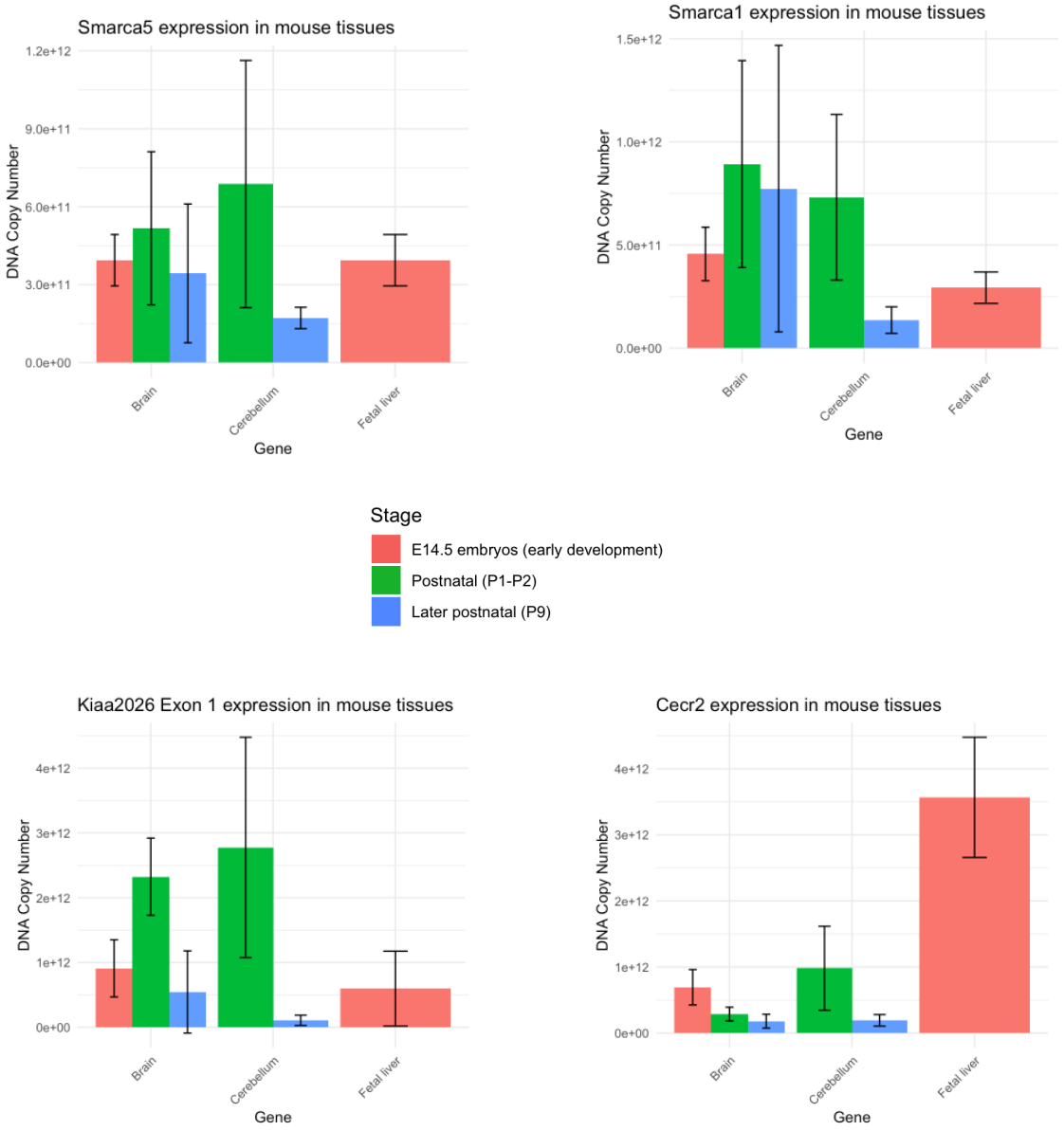


**Fig. 23 | Gene expression profiles of Smarca1, Smarca5, Kiaa2026 Exon 1 and Cecr2 across brain, cerebellum, and fetal liver at different developmental stages.** Embryonal stages were depicted in red, postnatal days 1-2 were represented by green, and postnatal day 9 was shown in blue.

During the transition from postnatal day 2 (P2) to postnatal day 9 (P9), there is a consistent decrease in expression levels observed for *Smarca1, Smarca5, CECR2, and Kiaa2026* genes

in the cerebellum. This declining trend suggests a broader developmental regulation or pattern associated with the gene expression dynamics during this stage of cerebellar development. The decreasing trend across multiple genes indicates a potential coordinated regulation or shared regulatory mechanism influencing their expression during postnatal development in the cerebellum.

Across genes *Smarca1*, *Smarca5*, *and Kiaa2026*, there is a consistent decreasing trend in expression levels as the brain transitions from P2 to E14.5 and further to P9. This declining trend suggests a potential developmental regulation or coordinated modulation of these genes' expression patterns during brain maturation from embryonic to postnatal stages.

Both the *Kiaa2026* and *Smarca1* genes consistently show lower levels of expression in the fetal liver that implies a significant difference in expression levels between these two tissues, suggesting a distinct regulatory landscape or developmental role for these genes in the fetal liver. Conversely, both CECR2 and Smarca5 genes consistently demonstrate higher levels of expression in the fetal liver, indicating a notable increase compared to other tissues, which may suggest unique developmental roles for these genes in this tissue.

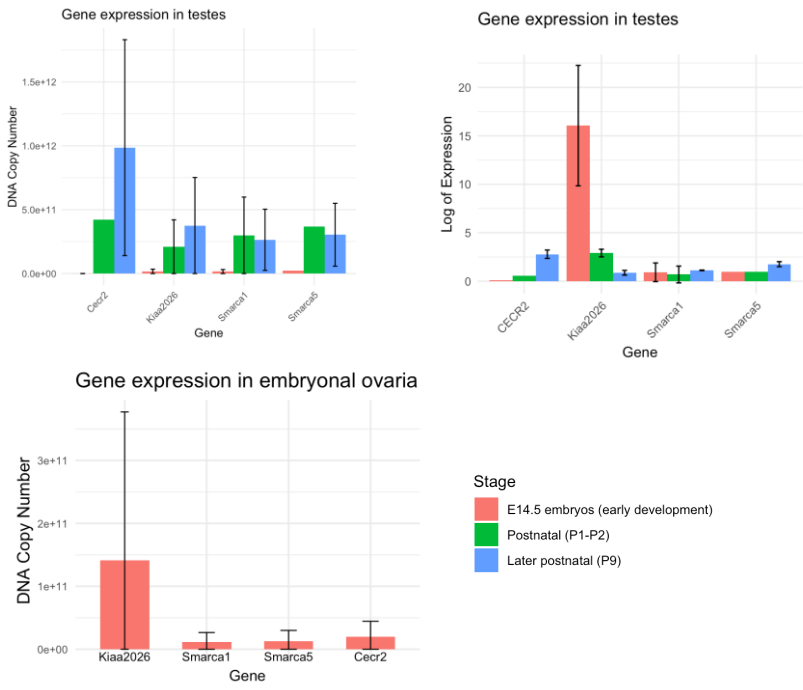


**Fig. 24 | Gene expression profiles of Smarca1, Smarca5, Kiaa2026 AND Cecr2 across testes at different developmental stages and embryonal ovaria.** The quantitative analysis of RT-qPCR is shown on the left image for testes while the right image presents qualitative analysis. Genes for normalization included housekeeping RNAs *Hprt1* and *Gapdh*. Embryonal stages are depicted in red, postnatal days 1-2 were represented by green, and postnatal day 9 is shown in blue.

The expression levels of *Kiaa2026* in the testes have been observed to show a significant decrease as development progresses from E14.5 to P2 and then to P9 when normalized against *Hprt1* and *Gapdh*. This consistent decreasing trend across developmental stages suggests a potential regulatory pattern or developmental modulation influencing *Kiaa2026* gene expression during testicular development from the embryonic stage to postnatal stages. The comparison between P2 and P9 displayed no significant difference, implying relative stability in expression levels at these two postnatal stages in the testes.

There has been a trend observed for Smarca1 and Smarca5 in the testes from E14.5 to P2 to P9: The ANOVA results did not indicate significant differences in log expression levels of Smarca1 and Smarca5 among the developmental stages in the testes. Additionally, comparisons between E14.5 and both P2 and P9 did not reveal significant differences for Smarca1 and Smarca5. The lack of significant differences across these stages suggests a trend of stability or no substantial change in log expression levels of *Smarca1* and *Smarca5* in the testes from the embryonic stage to both postnatal stages. This trend implies a consistent level of expression for these genes during testicular development across the studied stages, without notable variations or alterations in their expression patterns.

*Cecr2* displays a noticeable trend in the testes at stage P9, with a slight increase in expression levels compared to other stages. In contrast, both Smarca1 and Smarca5 genes maintain relatively consistent at this developmental stage.

The expression pattern of *Kiaa2026* presents an intriguing contrast across different embryonic tissues. In embryonal gonads, both in the testes and ovaries, *Kiaa2026* exhibits a notable state of overexpression. This heightened expression suggests a potentially pivotal role for Kiaa2026 in the developmental processes or specialized functions within these gonadal tissues during embryonic stages. Interestingly, when examining *Kiaa2026* expression in the fetal liver, a different trend emerges. Here, the expression pattern of *Kiaa2026* mirrors that of Smarca1, implying a similarity or resemblance between the expression dynamics of these two genes within the context of fetal liver.

The resemblance between *Kiaa2026* and *Smarca1* expression patterns in the fetal liver could suggest a potential functional or regulatory correlation. Understanding these contrasting and similar expression patterns in different tissues might provide valuable insights into the diverse roles and regulatory mechanisms governing Kiaa2026 in distinct embryonic and fetal tissues.

## 6.3 Interaction partners of KIAA2026

This chapter discusses three critical experimental techniques: co-immunoprecipitation, western blotting and mass spectrometry, essential for understanding and confirming interactions between proteins. It focuses on exploring potential interactions between CECR2, SMARCA5, and various domains of KIAA2026 using Co-IP assays combined with western blot analyses. Co-IP is a reliable method for isolating protein complexes formed by specific interactions. This study aims to elucidate and validate potential interactions among these proteins by using antibodies targeting DNA Topoisomerase 2A and Topoisomerase 2B, SNF2h/ISWI, FLAG and Strep II Tag. HEK293 cells underwent transfection with sequential plasmids (Table 7). To evaluate the success of transfection the presence of GFP (Green Fluorescent Protein) was measured using fluorescent microscopy (Fig.25).

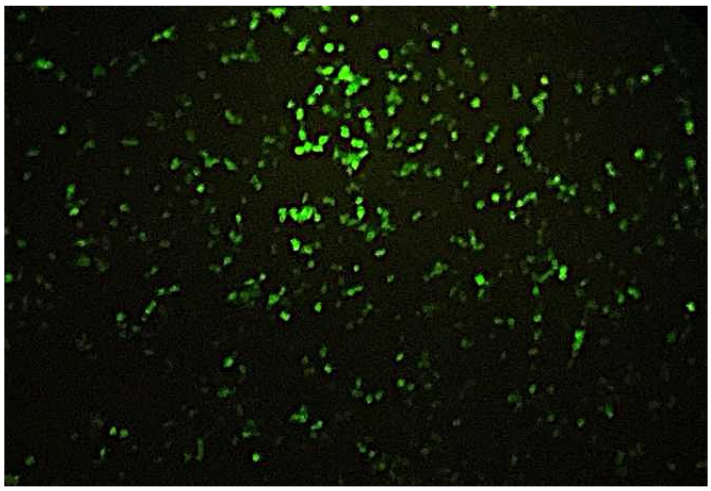

**Fig. 25 | HEK293 cells expressing GFP.**

Table 7: Plasmids for HEK293 transfection.

| **Plasmid Name:** |
|---|
| pGFP |
| pSBtet_SF-hSMARCA5_P2A_dsRed2 |
| pSBtet_SF-hCECR2_P2A_dsRed2 |
| pcDNA3.1-FlagStrepTag-mKIAA2026 $^{1-195}$ |
| pcDNA3.1-FlagStrepTag-mKIAA2026 $^{1-757}$ |
| pcDNA3.1-FlagStrepTag-mKIAA2026 $^{1-895}$ |
| pcDNA3.1-FlagStrepTag-mKIAA2026 $^{195-757}$ |
| pcDNA3.1-FlagStrepTag-mKIAA2026 $^{196-895}$ |

Following the Western Blot procedure, the membrane was stained with Ponceau S to assess the transfer process efficiency (Fig.26). The application of Ponceau S stain resulted in distinct, well-defined bands with uniform staining across the membrane. This suggests an even protein concentration across lanes, indicating a successful transfer and protein preparation.

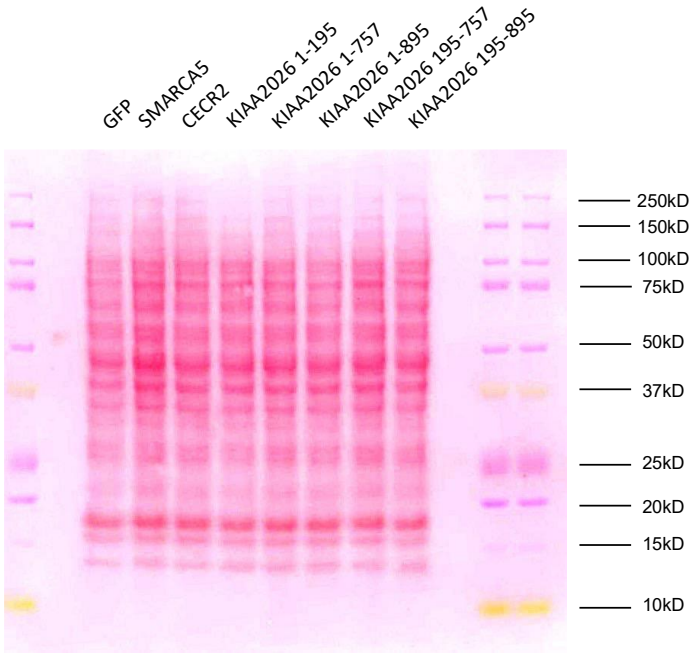


**Fig. 26 | Membrane stained with Ponceau S.**

The first step involved incubating the membrane with the Strep II Tag antibody to verify the presence and pinpoint the location of specific proteins: SMARCA5, CECR2, KIAA2026$^{1\text{-}195}$, KIAA2026$^{1\text{-}189}$ and KIAA2026$^{195\text{-}895}$. This approach facilitated visualization and localization of these proteins within the membrane. Upon closer examination using co-immunoprecipitation techniques, all five proteins were identified with noticeable expression levels. Notably, SMARCA5 and KIAA2026 $^{1\text{-}195}$ showed clear overexpression compared to other investigated proteins.

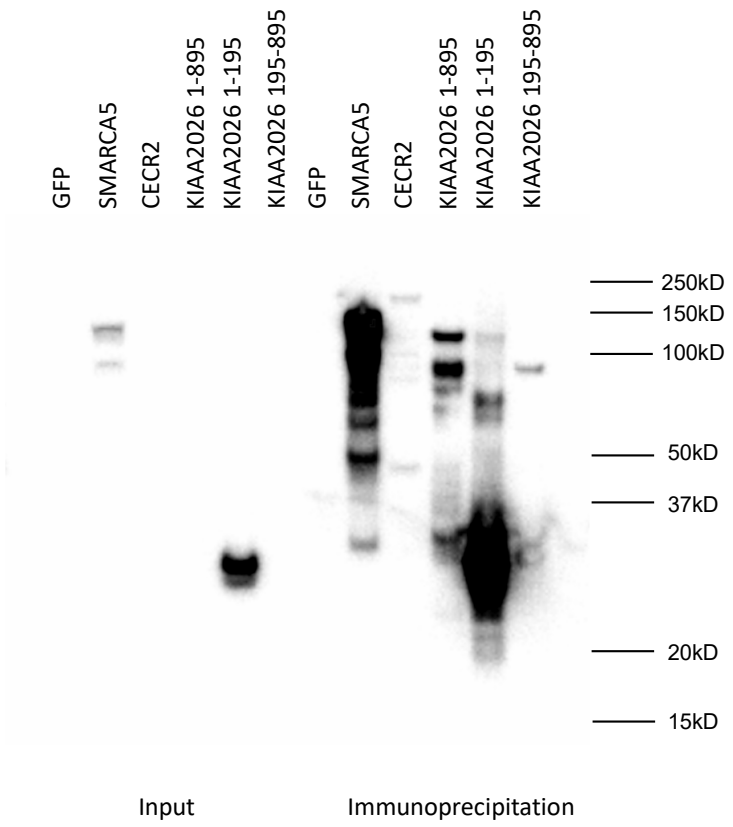


**Fig. 27 | Co-immunoprecipitation showing interaction with Strep II Tag.**

Subsequently, mass spectrometry was employed to investigate potential interaction partners of KIAA2026, using IgG as a control in the study. Specifically, it involved the following plasmids for overexpression in HEK293 cells:

pcDNA3.1-FlagStrepTag-mKIAA2026$^{1\text{-}195}$,

pcDNA3.1-FlagStrepTag-mKIAA2026$^{1\text{-}195}$ + Trichostatin (a selective HDAC inhibitor),

pcDNA3.1-FlagStrepTag-mKIAA2026$^{1\text{-}195}$ + Selisistat (EX527, a sirtuin inhibitor),

pcDNA3.1-FlagStrepTag-mKIAA2026$^{1\text{-}895}$,

pcDNA3.1-FlagStrepTag-mKIAA2026$^{196\text{-}895}$.

Table 8: Top 50 Genes Identified by Max Intensity in Mass Spectrometry Analysis.

| | Control | 1-894 | 195-894 | 1-195 CTRL | 1-195 Trichostatin | 1-195 Ex527 |
|---|---|---|---|---|---|---|
| DDX50 | 17 | 22,1443 | 17 | 24,1964 | 21,2653 | 24,0403 |
| TOP2B | 17 | 21,1367 | 17 | 22,9956 | 19,8829 | 21,4548 |
| LAS1L | 17 | 20,9307 | 17 | 22,7894 | 20,5736 | 22,0678 |
| SSR3 | 17 | 19,8107 | 17 | 21,2543 | 20,6994 | 20,9785 |
| PRR4 | 17 | 19,6946 | 17 | 21,1925 | 21,4688 | 20,7727 |
| ZNF280 | 17 | 19,2155 | 17 | 21,6887 | 17 | 20,9792 |

| | | | | | | |
|---|---|---|---|---|---|---|
| HDAC6 | 17 | 19,0002 | 17 | 21,1019 | 17 | 19,7834 |
| RFC1 | 17 | 18,9996 | 17 | 20,9292 | 20,3448 | 20,3509 |
| RPRD2 | 20,2313 | 21,9579 | 20,0599 | 23,5885 | 21,7325 | 23,2078 |
| SKI | 17 | 20,8551 | 19,0544 | 20,6919 | 21,3506 | 17 |
| DIMT1 | 17 | 18,5531 | 17 | 20,8987 | 18,9958 | 21,6986 |
| GTPBP4 | 17 | 18,5179 | 17 | 21,8299 | 17 | 17 |
| CENPB | 17 | 18,262 | 17 | 20,9321 | 17 | 20,8053 |
| POLR2B | 21,9245 | 23,0779 | 21,4596 | 25,959 | 23,4149 | 24,8384 |
| CPSF1 | 17 | 20,3302 | 19,1868 | 21,8428 | 19,3254 | 20,121 |
| POLR2G | 17 | 17,9927 | 17 | 22,7169 | 19,2953 | 22,3347 |
| POLR2A | 21,1521 | 22,1494 | 21,2099 | 25,4415 | 22,9715 | 24,3928 |
| TOP2A | 17 | 17,8529 | 17 | 20,0414 | 18,1492 | 19,2075 |
| PNO1 | 17 | 20,6583 | 19,9389 | 23,2886 | 20,4535 | 21,307 |
| H4 | 31,1511 | 31,8684 | 30,8675 | 33,899 | 31,5667 | 32,8078 |
| LSM12 | 17 | 22,7253 | 22,0811 | 23,4805 | 22,3902 | 21,7757 |
| H2A.V, H2A.Z | 26,7701 | 27,399 | 25,6371 | 28,7813 | 26,9684 | 28,4127 |
| PRRC2A | 20,935 | 21,561 | 20,6646 | 21,5556 | 20,1157 | 19,9183 |
| RBM10 | 18,2318 | 18,7025 | 17 | 20,9942 | 19,0495 | 20,0614 |
| TSR1 | 20,0654 | 20,5252 | 19,0642 | 24,5052 | 20,5959 | 22,5688 |
| RBM14 | 23,4712 | 24,6104 | 24,1622 | 25,1128 | 24,4665 | 24,6433 |
| FBL | 20,8419 | 22,1607 | 21,7561 | 23,6281 | 24,0785 | 23,4532 |
| H2A | 32,3559 | 32,7269 | 31,4662 | 34,3802 | 32,5971 | 34,0166 |
| DBF4B | 24,1217 | 24,4561 | 17 | 24,4118 | 24,2669 | 25,3225 |
| H3F3A | 24,3892 | 24,6833 | 24,405 | 27,6505 | 25,5076 | 23,3543 |
| H3 | 29,9985 | 30,2528 | 28,4775 | 32,0132 | 30,0144 | 31,3038 |
| H2B | 31,2151 | 31,4504 | 30,5705 | 33,9659 | 31,5906 | 30,9246 |
| HIST2H2AB | 17 | 24,4392 | 24,2073 | 25,683 | 25,0615 | 25,7141 |
| BYSL | 18,8199 | 20,0449 | 19,8462 | 22,3417 | 17 | 20,353 |
| H2A | 26,3022 | 26,4755 | 25,8002 | 30,6578 | 28,0521 | 28,5211 |
| PDCD4 | 21,895 | 22,036 | 21,7558 | 23,2318 | 17 | 21,6956 |
| PAF1 | 23,1191 | 23,2185 | 22,5013 | 25,9665 | 22,5451 | 25,4247 |
| RPRD1B | 23,1784 | 23,2128 | 22,5658 | 25,5455 | 22,801 | 24,6842 |
| WDR18 | 20,5985 | 20,6016 | 17 | 24,2484 | 21,8144 | 23,0802 |
| LOXHD1 | 17 | 25,0353 | 17 | 17 | 17 | 17 |
| TEX10 | 17 | 17 | 17 | 23,8933 | 17 | 23,1464 |
| SRPX | 17 | 17 | 17 | 23,772 | 17 | 17 |
| TMEM43 | 17 | 17 | 17 | 23,0573 | 23,0154 | 23,1437 |
| POLR2I | 17 | 17 | 17 | 22,7021 | 17 | 17 |
| CHD1 | 17 | 17 | 17 | 22,468 | 17 | 22,5718 |

| | | | | | | |
|---|---|---|---|---|---|---|
| SFN | 17 | 17 | 17 | 17 | 22,2774 | 22,4891 |
| TRIM26 | 17 | 17 | 17 | 17 | 17 | 22,4863 |
| SLURP1 | 17 | 17 | 17 | 17 | 22,0046 | 22,4406 |
| SKP1 | 17 | 17 | 17 | 22,4079 | 22,2987 | 20,5159 |
| HMGA1 | 17 | 17 | 17 | 22,2936 | 20,6472 | 20,2054 |

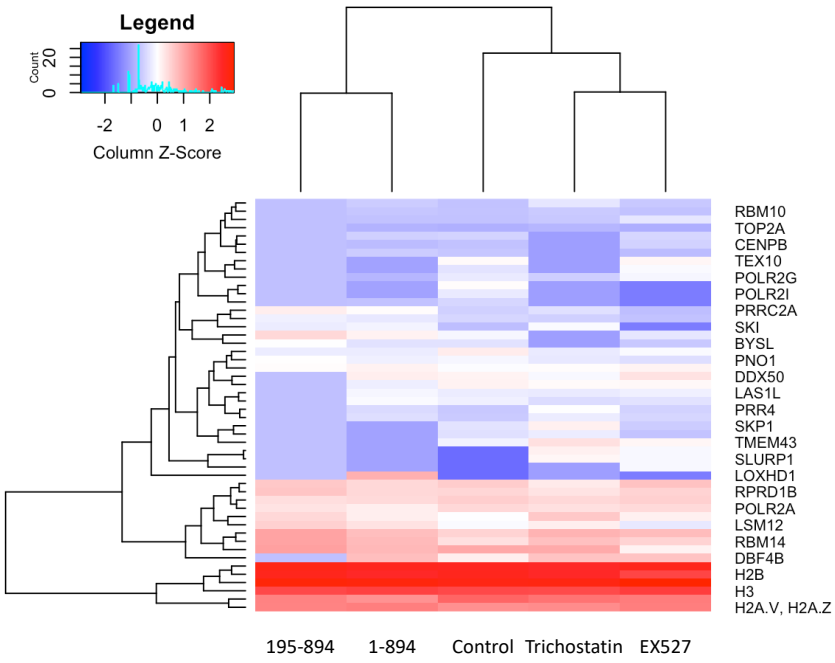


**Fig. 28 | Heat map showing potential interaction partners of KIAA2026.**

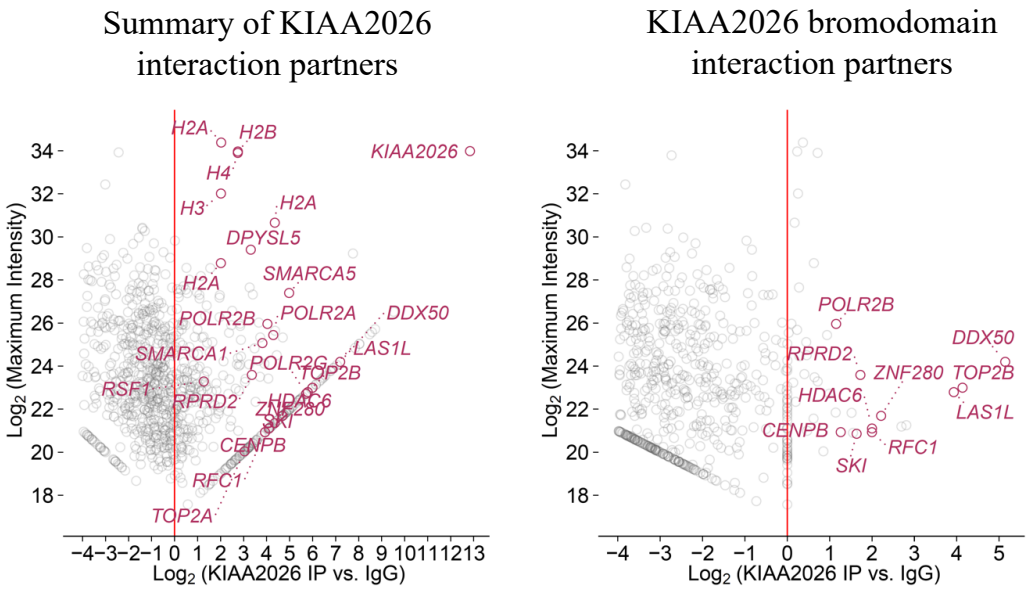


**Fig. 29 | KIAA2026 interaction partners by overexpression in HEK293 cell lines.**

Samples containing SMARCA5, CECR2, KIAA2026$^{1-195}$, KIAA2026$^{1-757}$, KIAA2026$^{1-895}$, KIAA2026$^{195-757}$, and KIAA2026 $^{195-895}$ were incubated with the Flag antibody (Fig. 30). This step aimed to validate the process of immunoprecipitation and precisely determine the localization of these specific proteins. However, it's important to note that the antibody was unable to capture all the targeted proteins in the sample. Despite its limitations, the results did reveal a significant finding: an overexpression pattern related to the approximate size of 35kD for the KIAA2026$^{1-195}$ protein was detected.

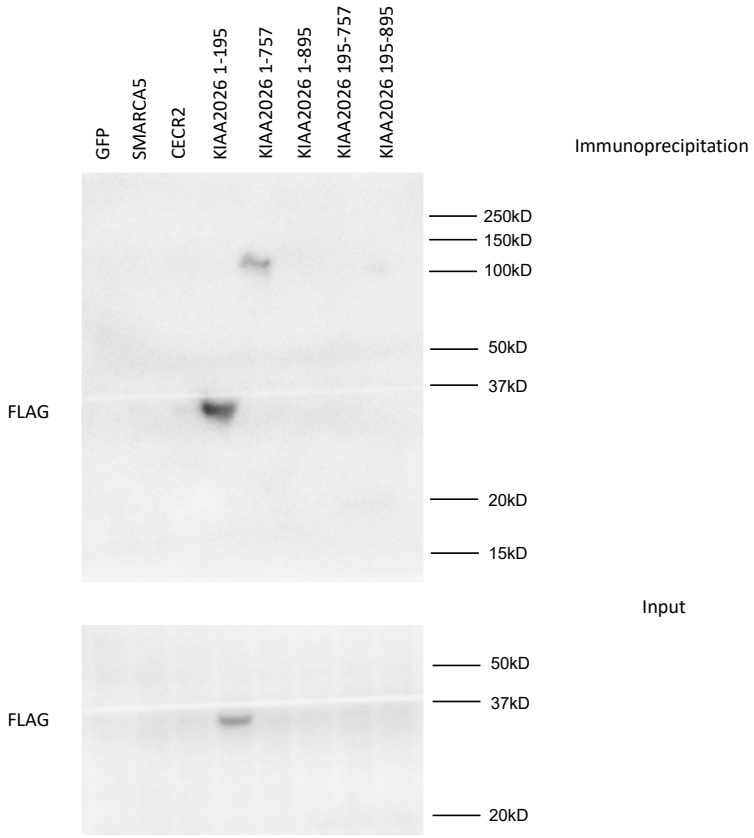


**Fig. 30 | Co-immunoprecipitation showing interaction with FLAG.**

Samples containing SMARCA5, CECR2, KIAA2026 $^{1-195}$, KIAA2026 $^{1-757}$, KIAA2026 $^{1-895}$, KIAA2026 $^{195-757}$, and KIAA2026 $^{195-895}$ were incubated with the SMARCA5 antibody to explore potential interactions among these proteins (Fig. 31). The results revealed a confirmed interaction between SMARCA5 antibody and SMARCA5 protein as well as CECR2 protein. This outcome aligns with the known partnership between CECR2 and SMARCA5, validating the experimental approach accuracy. Interestingly, the interaction study showed significant interactions in the co-immunoprecipitation assay within the KIAA2026$^{195-895}$ fragment, strongly indicating its potential involvement in binding Smarca5. Additionally, observations

revealed co-immunoprecipitation at a lesser magnitude, yet still noteworthy, within both the KIAA2026 $^{1-757}$ and KIAA2026 $^{1-895}$ fragments. Further analysis highlighted a much subtler but noticeable interaction between Smarca5 and the KIAA2026 $^{195-757}$ fragment. However, no evidence of interaction bromodomain (KIAA2026 $^{1-195}$) was found based on this study's results.

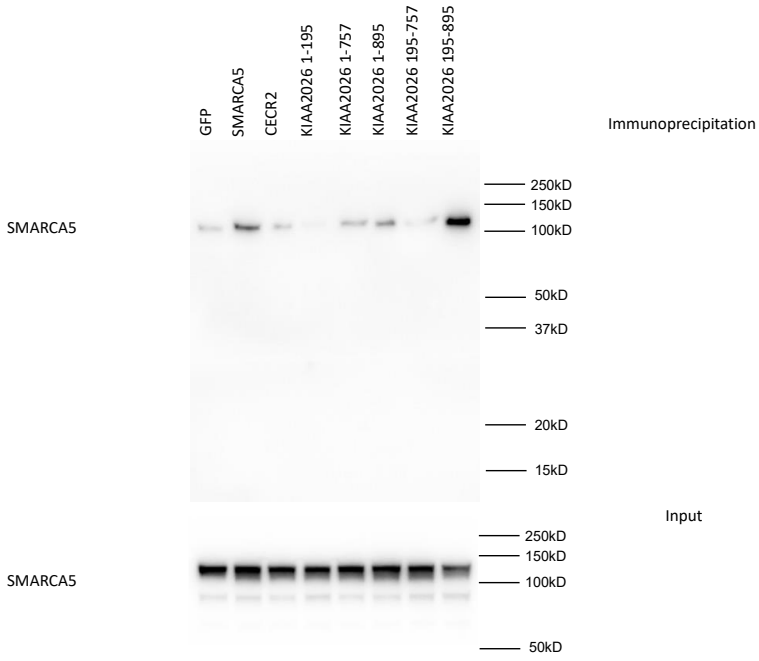


**Fig. 31 | Co-immunoprecipitation showing interaction with SMARCA5.**

Staining using a combination of Topoisomerase IIA and Topoisomerase IIB antibody revealed valuable insights into the interaction profiles between previous proteins and Topoisomerase II (Fig. 32). A strong affinity was observed between SMARCA5 and the Topoisomerase II, indicating robust interaction. Additionally, notable interactions were detected between SMARCA5 and the KIAA2026 $^{195-757}$ fragment, as well as moderate interaction levels within the KIAA2026 $^{1-757}$ and KIAA2026 $^{1-895}$ fragments. Conversely, no detectable interactions were observed with the KIAA2026 $^{195-895}$, KIAA2026 $^{1-195}$, or CECR2 proteins.

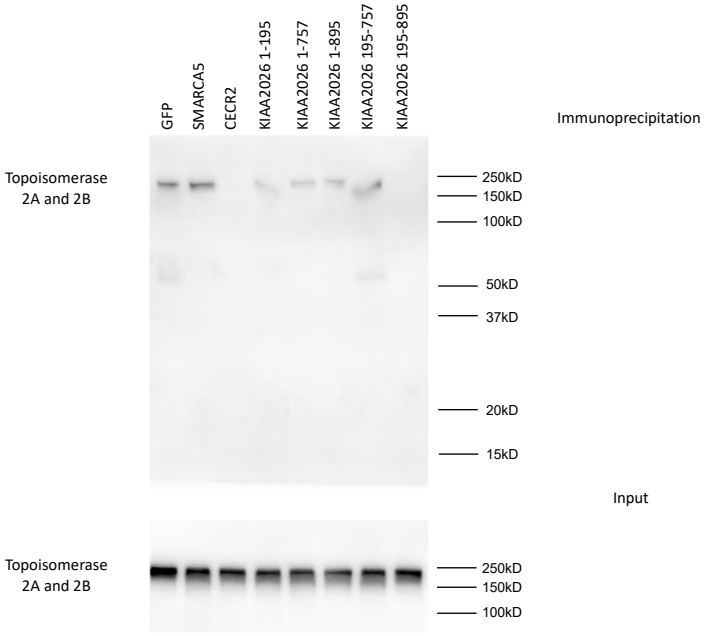


**Fig. 32 | Co-immunoprecipitation showing interaction with Topoisomerase II.**

# 7 Discussion

SMARCA5, an ISWI family member, contributes significantly to nucleosome spacing impacting hematopoiesis, spermatogenesis and brain development, and its dysregulation is implicated in multiple human cancers, suggesting its conserved role across diverse organisms and highlighting the potential to elucidate tissue-specific functions and chromatin regulation via investigation of its interaction partners in mammalian cell models (Bomber *et al*., 2023). The main goal of this work was to investigate and validate potential new interaction partners of Smarca5. Our laboratory performed mass spectrometry analysis, revealing a likely connection between Smarca5 and a previously uncharacterized protein called Brd10 (also known as Kiaa2026). Kiaa2026's own expression pattern in neuronal and glial cells, along with its presence in germ cells and testes (spermatocytes and spermatogonia) indicated a strong overlap between the expression profiles of Smarca5 and Kiaa2026. This preliminary genetic interaction was further supported by the presence of DDT-WHIM1-WHIM2 domains, which is a feature found in all ISWI interaction partners, including Kiaa2026.

The highly conserved primary structure of Kiaa2026 across various domains implies its significance and suggests its potential functional importance in diverse biological processes. This thesis aimed to confirm the interaction between KIAA2026 and SMARCA5, to identify specific domains of Kiaa2026 protein responsible for binding to Smarca5. The study also explored other proteins interacting with Kiaa2026, including its non-canonical bromodomain, through co-immunoprecipitation methods. Furthermore, the thesis compared the tissue-specific expression pattern of *Kiaa2026* with the expression profiles of ISWI chromatin remodelers and established Smarca5-Kiaa2026 genetic interaction using RT-PCR.

The DDT-WHIM1-WHIM2 sequence functions as an ISWI binding module, allowing interactions with ISWI ATPase across all domains of life, as proteins containing the DDT domain can attach to the SLIDE domain of ISWI ATPase (*e.g.* Smarca5) (Dong *et al*., 2013). The presence of this domain in Kiaa2026 suggests a similar function. Additionally, WHIM motifs are believed to interact with nucleosomal linker DNA and the SLIDE domain present in ISWI proteins. Deletion mapping studies have suggested that within the BAZ2B protein, the conserved BAZ region, which overlaps with WHIM2, is crucial for binding Smarca5 (Aravind and Iyer, 2012). Overall, DDT-WHIM1-WHIM2 domains act like a "protein ruler", arranging nucleosome spacing alongside an ISWI ATPase. Furthermore, the C-terminus of the ISWI binding module contains a highly conserved region whose function remains unknown. Designed plasmids included those with only the bromodomain, solely the DDT-WHIM1-

WHIM module, both the Bromodomain and DDT-WHIM1-WHIM module, as well as options with or without IBM-C.

As *Kiaa2026* was detected in both germ and neuronal cells, RT-PCR analysis was conducted to examine mRNA expression in various tissues of mice, including the testes, ovaries, brain, and cerebellum. Fetal liver, known for its high expression of Smarca5, was also included in the study (Kokavec *et al*., 2017). Given the distinct expression patterns of *Smarca1* and *Smarca5* across different developmental stages, the investigation focused on three specific stages: embryonal stage 14.5, postnatal day 1 or 2, and postnatal day 9. The findings revealed a notable trend in *Kiaa2026* expression, peaking at postnatal day 2 and gradually decreasing at the embryonal stage and postnatal day 9 in both the brain and cerebellum.

Intriguingly, the expression levels of *Kiaa2026* in brain and cerebellum at each stage closely mirrored those of *Smarca1* and *Smarca5*, suggesting a potential co-regulation or functional interrelation between these genes. Interestingly, both Smarca1 and Smarca5 regulates neurodevelopment, with Smarca1 pathogenic variants leading to intellectual disability or developmental delay and *Smarca5* deficiency resulting in severe cerebellar and forebrain hypoplasia (Alvarez-Saavedra *et al*., 2016; Picketts *et al*., 2023).

The consistent expression patterns observed across these genes suggest a potential coordinated involvement in various biological processes or co-expression throughout developmental stages. Interestingly, while Cecr2 levels are notably high during embryonal stage 14.5, their sharp decline into postnatal stages emphasizes the significance of this gene in embryonal brain development (Fairbridge *et al.*, 2010).

The observed low expression levels of *Kiaa2026* and *Smarca1* in fetal liver contrast with the higher expression of *Smarca5* and *Cecr2*. Previous research has underscored the significance of Cecr2 and Smarca5 in hematopoiesis, aligning with these findings (Ding *et al*., 2021). Consequently, it may be inferred that neither Smarca1 nor Kiaa2026 play a critical role in the hematopoietic process.

The analysis of *Kiaa2026* RNA expression revealed a notable increase in early embryonal testes, followed by a significant decrease in later postnatal stages. This was accompanied by enhanced embryonal expression in ovaria, suggesting potential involvement in early gonadal maturation and gonadal differentiation during embryogenesis. Furthermore, the trend in *Cecr2* expression levels, lower during the embryonal stage and increased on subsequent postnatal days 2 and 9, appear to be consistent with its regulatory role in gene expression throughout spermatogenesis.

Overall, the newfound connection between Kiaa2026 and Smarca5 hints at a significant interaction pivotal for neurodevelopment and particularly crucial during gametogenesis, highlighting Kiaa2026's role in the early development of testes. Understanding the intricacies of this interaction could illuminate crucial mechanisms dictating cellular differentiation, especially in the context of neural and gonad development. Further investigation into the specific dynamics and functions of this partnership may shed light on how these genes orchestrate pathways crucial for early brain and reproductive system development.

The validation of the Kiaa2026 and Smarca5 interaction and the identification of protein interactions involving Smarca5, Cecr2, and various domains of Kiaa2026 were conducted by Western blot and co-immunoprecipitation. Smarca5 interaction with CECR2 was confirmed through co-immunoprecipitation, consistent with earlier research (Thompson *et al*., 2012). Furthermore, evidence suggests that Kiaa2026 might be a Smarca5 binding partner, potentially via the ISWI binding module and specifically involving the IBM-C domain. It is noteworthy that as expected, the bromodomain does not appear to bind Smarca5. This highlights the need for additional investigation into the ability of the IBM-C domain to bind to the SLIDE domain. Future research might involve exploring domain-specific functions, investigating conserved domain functions and specific protein interactions. Additionally, gaining a deeper insight into the IBM-C domain interaction with the ISWI proteins could enrich our understanding of protein interactions, as well as their impact on chromatin regulation.

Studies have showcased the relationship between BAZ proteins and Topoisomerases. The BAZ1B-SMARCA5 complex is associated with the functionality of Topoisomerase I, while BAZ2A-SMARCA5 interacts with Topoisomerase IIA (Ribeyre *et al*., 2016; Dalcher *et al*., 2020; Roganowicz *et al*., 2023). To explore the potential link between Kiaa2026 and Topoisomerase II, co-immunoprecipitation experiments were conducted. These experiments reaffirmed the interaction between Smarca5 and Topoisomerase II, aligning with prior findings. However, there was no observed interaction with the CECR2 protein.

Interestingly, an interaction was revealed between the DDT-WHIM1-WHIM domains of Kiaa2026 and Topoisomerase, irrespective of the presence of the Bromodomain. This discovery was unexpected given previous studies indicating that certain Bromodomain-containing proteins like BPTF, BRD2, and SP140 can interact with Topoisomerases, influencing their significance in tumor development (Kim *et al*., 2019; Tyutyunyk-Massey *et al*., 2021; Amatullah *et al*., 2022). This unexpected interaction between Topoisomerase II and Kiaa2026 protein might occur directly or potentially through Smarca5.

Our working hypothesis consisted of an idea that KIAA2026 formed an interaction with SMARCA5, as previously identified by mass spectrometry analysis. The co-localization of KIAA2026 in neuronal and glial cells, along its shared expression profile with Smarca5, supported this proposed interaction. The primary objective of the study was to validate this interaction, identify the specific binding region involved, conduct an exploration of additional protein interactions utilizing co-immunoprecipitation methods, and perform a comparative analysis of tissue-specific expression patterns alongside ISWI chromatin remodelers.

In summary, Kiaa2026 has been identified as a Smarca5 interaction partner through its ISWI-binding module, where its Bromodomain appears to recognize acetylated histones. This finding strongly implies the involvement of Kiaa2026 in chromatin remodeling processes, particularly in embryonic testes and brain tissues. Moreover, its association with Topoisomerase II suggests a potential role in DNA damage repair mechanisms and DDR-mediated (and physiological) transcription during development. Further investigations into its interaction with Topoisomerase I and experiments using histone-acetylase inhibitors could offer deeper insights into the behavior of the bromodomain. It's worth noting that all gene expression analyses were conducted in wild-type mice; thus, repeating these experiments in Kiaa2026 knock-out mice could yield valuable comparative data. Additionally, refining mass spectrometry experiments could potentially reveal additional interaction partners of Kiaa2026 with higher precision.

# 8 Conclusions

- BRD10 (Kiaa2026) has been confirmed as a Smarca5 interaction partner via its ISWI-binding module, with its IBM-C domain specifically showing affinity for Smarca5

- This discovery strongly indicates BRD10 (Kiaa2026) engagement in chromatin remodeling in embryonic testes and brain tissues

- Its interaction with Topoisomerase II hints at a plausible involvement in DNA repair processes

# 9 References


Alkhatib, S. G., & Landry, J. W. (2011). The Nucleosome Remodeling Factor. *FEBS Letters*, *585*(20), 3197–3207. https://doi.org/10.1016/j.febslet.2011.09.003

Alvarez-Saavedra, M., De Repentigny, Y., Lagali, P. S., Raghu Ram, E. V. S., Yan, K., Hashem, E., Ivanochko, D., Huh, M. S., Yang, D., Mears, A. J., Todd, M. A. M., Corcoran, C. P., Bassett, E. A., Tokarew, N. J. A., Kokavec, J., Majumder, R., Ioshikhes, I., Wallace, V. A., Kothary, R., … Picketts, D. J. (2014). Snf2h-mediated chromatin organization and histone H1 dynamics govern cerebellar morphogenesis and neural maturation. *Nature Communications*, *5*(1), 4181. https://doi.org/10.1038/ncomms5181

Alvarez-Saavedra, M., De Repentigny, Y., Yang, D., O'Meara, R. W., Yan, K., Hashem, L. E., Racacho, L., Ioshikhes, I., Bulman, D. E., Parks, R. J., Kothary, R., & Picketts, D. J. (2016). Voluntary Running Triggers VGF-Mediated Oligodendrogenesis to Prolong the Lifespan of Snf2h-Null Ataxic Mice. *Cell Reports*, *17*(3), 862–875. https://doi.org/10.1016/j.celrep.2016.09.030

Alvarez-Saavedra, M., Yan, K., De Repentigny, Y., Hashem, L. E., Chaudary, N., Sarwar, S., Yang, D., Ioshikhes, I., Kothary, R., Hirayama, T., Yagi, T., & Picketts, D. J. (2019). Snf2h Drives Chromatin Remodeling to Prime Upper Layer Cortical Neuron Development. *Frontiers in Molecular Neuroscience*, *12*, 243. https://doi.org/10.3389/fnmol.2019.00243

Amatullah, H., Fraschilla, I., Digumarthi, S., Huang, J., Adiliaghdam, F., Bonilla, G., Wong, L. P., Rivard, M.-E., Beauchamp, C., Mercier, V., Goyette, P., Sadreyev, R. I., Anthony, R. M., Rioux, J. D., & Jeffrey, K. L. (2022). Epigenetic reader SP140 loss of function drives Crohn's disease due to uncontrolled macrophage topoisomerases. *Cell*, *185*(17), 3232-3247.e18. https://doi.org/10.1016/j.cell.2022.06.048

Anosova, I., Melnik, S., Tripsianes, K., Kateb, F., Grummt, I., & Sattler, M. (2015). A novel RNA binding surface of the TAM domain of TIP5/BAZ2A mediates epigenetic regulation of rRNA genes. *Nucleic Acids Research*, *43*(10), 5208–5220. https://doi.org/10.1093/nar/gkv365

Aravind, L., & Iyer, L. M. (2012). The HARE-HTH and associated domains: Novel modules in the coordination of epigenetic DNA and protein modifications. *Cell Cycle*, *11*(1), 119–131. https://doi.org/10.4161/cc.11.1.18475

Arumugam, K., Shin, W., Schiavone, V., Vlahos, L., Tu, X., Carnevali, D., Kesner, J., Paull, E. O., Romo, N., Subramaniam, P., Worley, J., Tan, X., Califano, A., & Cosma, M. P. (2020). The Master Regulator Protein BAZ2B Can Reprogram Human Hematopoietic Lineage-Committed Progenitors into a Multipotent State. *Cell Reports*, *33*(10), 108474. https://doi.org/10.1016/j.celrep.2020.108474

Aydin, Ö. Z., Vermeulen, W., & Lans, H. (2014). ISWI chromatin remodeling complexes in the DNA damage response. *Cell Cycle*, *13*(19), 3016–3025. https://doi.org/10.4161/15384101.2014.956551

Banting, G. S., Barak, O., Ames, T. M., Burnham, A. C., Kardel, M. D., Cooch, N. S., Davidson, C. E., Godbout, R., McDermid, H. E., & Shiekhattar, R. (2005). CECR2, a protein involved in neurulation, forms a novel chromatin remodeling complex with SNF2L. *Human Molecular Genetics*, *14*(4), 513–524. https://doi.org/10.1093/hmg/ddi048

Barisic, D., Stadler, M. B., Iurlaro, M., & Schübeler, D. (2019). Mammalian ISWI and SWI/SNF selectively mediate binding of distinct transcription factors. *Nature*, *569*(7754), 136–140. https://doi.org/10.1038/s41586-019-1115-5

Barnett, C., & Krebs, J. E. (2011). WSTF does it all: A multifunctional protein in transcription, repair, and replicationThis paper is one of a selection of papers published in a Special Issue entitled 31st Annual International Asilomar Chromatin and Chromosomes Conference, and has undergone the Journal's usual peer review process. *Biochemistry and Cell Biology*, *89*(1), 12–23. https://doi.org/10.1139/O10-114

Bomber, M. L., Wang, J., Liu, Q., Barnett, K. R., Layden, H. M., Hodges, E., Stengel, K. R., & Hiebert, S. W. (2023). Human SMARCA5 is continuously required to maintain nucleosome spacing. *Molecular Cell*, *83*(4), 507-522.e6. https://doi.org/10.1016/j.molcel.2022.12.018

Börner, K., Jain, D., Vazquez-Pianzola, P., Vengadasalam, S., Steffen, N., Fyodorov, D. V., Tomancak, P., Konev, A., Suter, B., & Becker, P. B. (2016). A role for tuned levels of nucleosome remodeler subunit ACF1 during Drosophila oogenesis. *Developmental Biology*, *411*(2), 217–230. https://doi.org/10.1016/j.ydbio.2016.01.039

Bortoluzzi, A., Amato, A., Lucas, X., Blank, M., & Ciulli, A. (2017). Structural basis of molecular recognition of helical histone H3 tail by PHD finger domains. *Biochemical Journal*, *474*(10), 1633–1651. https://doi.org/10.1042/BCJ20161053

Cavellán, E., Asp, P., Percipalle, P., & Farrants, A.-K. Ö. (2006). The WSTF-SNF2h Chromatin Remodeling Complex Interacts with Several Nuclear Proteins in Transcription. *Journal of Biological Chemistry*, *281*(24), 16264–16271. https://doi.org/10.1074/jbc.M600233200

Centore, R. C., Sandoval, G. J., Soares, L. M. M., Kadoch, C., & Chan, H. M. (2020). Mammalian SWI/SNF Chromatin Remodeling Complexes: Emerging Mechanisms and Therapeutic Strategies. *Trends in Genetics: TIG*, *36*(12), 936–950. https://doi.org/10.1016/j.tig.2020.07.011

Chen, S., Zhou, M., Dong, A., Loppnau, P., Wang, M., Min, J., & Liu, K. (2021). Structural basis of the TAM domain of BAZ2A in binding to DNA or RNA independent of methylation status. *Journal of Biological Chemistry*, *297*(6), 101351. https://doi.org/10.1016/j.jbc.2021.101351

Clapier, C. R., & Cairns, B. R. (2009). The biology of chromatin remodeling complexes. *Annual Review of Biochemistry*, *78*, 273–304. https://doi.org/10.1146/annurev.biochem.77.062706.153223

Corona, D. F. V. (2000). Two histone fold proteins, CHRAC-14 and CHRAC-16, are developmentally regulated subunits of chromatin accessibility complex (CHRAC). *The EMBO Journal*, *19*(12), 3049–3059. https://doi.org/10.1093/emboj/19.12.3049

Corona, D. F. V., & Tamkun, J. W. (2004). Multiple roles for ISWI in transcription, chromosome organization and DNA replication. *Biochimica et Biophysica Acta (BBA) - Gene Structure and Expression*, *1677*(1–3), 113–119. https://doi.org/10.1016/j.bbaexp.2003.09.018

Dalcher, D., Tan, J. Y., Bersaglieri, C., Peña-Hernández, R., Vollenweider, E., Zeyen, S., Schmid, M. W., Bianchi, V., Butz, S., Roganowicz, M., Kuzyakiv, R., Baubec, T., Marques, A. C., & Santoro, R. (2020). BAZ 2A safeguards genome architecture of ground-state pluripotent stem cells. *The EMBO Journal*, *39*(23), e105606. https://doi.org/10.15252/embj.2020105606

Dalle Vedove, A., Cazzanelli, G., Batiste, L., Marchand, J.-R., Spiliotopoulos, D., Corsi, J., D'Agostino, V. G., Caflisch, A., & Lolli, G. (2022). Identification of a BAZ2A-Bromodomain Hit Compound by Fragment Growing. *ACS Medicinal Chemistry Letters*, *13*(9), 1434–1443. https://doi.org/10.1021/acsmedchemlett.2c00173

Dawe, C. E., Kooistra, M. K., Fairbridge, N. A., Pisio, A. C., & McDermid, H. E. (2011). Role of chromatin remodeling gene *Cecr2* in neurulation and inner ear development. *Developmental Dynamics*, *240*(2), 372–383. https://doi.org/10.1002/dvdy.22547

Dehingia, B., Milewska, M., Janowski, M., & Pękowska, A. (2022). CTCF shapes chromatin structure and gene expression in health and disease. *EMBO Reports*, *23*(9), e55146. https://doi.org/10.15252/embr.202255146

Deindl, S., Hwang, W. L., Hota, S. K., Blosser, T. R., Prasad, P., Bartholomew, B., & Zhuang, X. (2013). ISWI Remodelers Slide Nucleosomes with Coordinated Multi-Base-Pair Entry Steps and Single-Base-Pair Exit Steps. *Cell*, *152*(3), 442–452. https://doi.org/10.1016/j.cell.2012.12.040

Dicipulo, R., Norton, K. A., Fairbridge, N. A., Kibalnyk, Y., Fox, S. C., Hornberger, L. K., & McDermid, H. E. (2021). Cecr2 mutant mice as a model for human cat eye syndrome. *Scientific Reports*, *11*(1), 3111. https://doi.org/10.1038/s41598-021-82556-y

Ding, Y., Wang, W., Ma, D., Liang, G., Kang, Z., Xue, Y., Zhang, Y., Wang, L., Heng, J., Zhang, Y., & Liu, F. (2021). Smarca5-mediated epigenetic programming facilitates fetal HSPC development in vertebrates. *Blood*, *137*(2), 190–202. https://doi.org/10.1182/blood.2020005219

Dirscherl, S. S., & Krebs, J. E. (2004). Functional diversity of ISWI complexes. *Biochemistry and Cell Biology*, *82*(4), 482–489. https://doi.org/10.1139/o04-044

Dluhosova, M., Curik, N., Vargova, J., Jonasova, A., Zikmund, T., & Stopka, T. (2014). Epigenetic Control of SPI1 Gene by CTCF and ISWI ATPase SMARCA5. *PLoS ONE*, *9*(2), e87448. https://doi.org/10.1371/journal.pone.0087448

Dong, J., Gao, Z., Liu, S., Li, G., Yang, Z., Huang, H., & Xu, L. (2013). SLIDE , The Protein Interacting Domain of Imitation Switch Remodelers, Binds DDT - D omain Proteins of Different Subfamilies in Chromatin Remodeling Complexes. *Journal of Integrative Plant Biology*, *55*(10), 928–937. https://doi.org/10.1111/jipb.12069

Eckey, M., Kuphal, S., Straub, T., Rümmele, P., Kremmer, E., Bosserhoff, A. K., & Becker, P. B. (2012). Nucleosome Remodeler SNF2L Suppresses Cell Proliferation and Migration and Attenuates Wnt Signaling. *Molecular and Cellular Biology*, *32*(13), 2359–2371. https://doi.org/10.1128/MCB.06619-11

Fairbridge, N. A., Dawe, C. E., Niri, F. H., Kooistra, M. K., King-Jones, K., & McDermid, H. E. (2010). *Cecr2* mutations causing exencephaly trigger misregulation of mesenchymal/ectodermal transcription factors. *Birth Defects Research Part A: Clinical and Molecular Teratology*, *88*(8), 619–625. https://doi.org/10.1002/bdra.20695

Feng, Y., Chen, S., Zhou, M., Zhang, J., Min, J., & Liu, K. (2022). Crystal structure of the BAZ2B TAM domain. *Heliyon*, *8*(7), e09873. https://doi.org/10.1016/j.heliyon.2022.e09873

Filarsky, M., Zillner, K., Araya, I., Villar-Garea, A., Merkl, R., Längst, G., & Németh, A. (2015). The extended AT-hook is a novel RNA binding motif. *RNA Biology*, *12*(8), 864–876. https://doi.org/10.1080/15476286.2015.1060394

Florescu, A.-M., Schiessel, H., & Blossey, R. (2012). Kinetic Control of Nucleosome Displacement by ISWI/ACF Chromatin Remodelers. *Physical Review Letters*, *109*(11), 118103. https://doi.org/10.1103/PhysRevLett.109.118103

Fyodorov, D. V., Blower, M. D., Karpen, G. H., & Kadonaga, J. T. (2004). Acf1 confers unique activities to ACF/CHRAC and promotes the formation rather than disruption of chromatin in vivo. *Genes & Development*, *18*(2), 170–183. https://doi.org/10.1101/gad.1139604

Goodwin, L. R., & Picketts, D. J. (2018). The role of ISWI chromatin remodeling complexes in brain development and neurodevelopmental disorders. *Molecular and Cellular Neuroscience*, *87*, 55–64. https://doi.org/10.1016/j.mcn.2017.10.008

Grüne, T., Brzeski, J., Eberharter, A., Clapier, C. R., Corona, D. F. V., Becker, P. B., & Müller, C. W. (2003). Crystal Structure and Functional Analysis of a Nucleosome Recognition Module of the Remodeling Factor ISWI. *Molecular Cell*, *12*(2), 449–460. https://doi.org/10.1016/S1097-2765(03)00273-9

He, J., Fu, L., & Li, Q. (2019). Rsf-1 regulates malignant melanoma cell viability and chemoresistance via NF-κB/Bcl-2 signaling. *Molecular Medicine Reports*. https://doi.org/10.3892/mmr.2019.10610

Hoffmeister, H., Fuchs, A., Erdel, F., Pinz, S., Gröbner-Ferreira, R., Bruckmann, A., Deutzmann, R., Schwartz, U., Maldonado, R., Huber, C., Dendorfer, A.-S., Rippe, K., & Längst, G. (2017). CHD3 and CHD4 form distinct NuRD complexes with different yet overlapping functionality. *Nucleic Acids Research*, *45*(18), 10534–10554. https://doi.org/10.1093/nar/gkx711

Ito, T., Tyler, J. K., & Kadonaga, J. T. (1997). Chromatin assembly factors: A dual function in nucleosome formation and mobilization? *Genes to Cells*, *2*(10), 593–600. https://doi.org/10.1046/j.1365-2443.1997.1500348.x

Jumper, J., & Hassabis, D. (2022). Protein structure predictions to atomic accuracy with AlphaFold. *Nature Methods*, *19*(1), 11–12. https://doi.org/10.1038/s41592-021-01362-6

Kim, J. J., Lee, S. Y., Gong, F., Battenhouse, A. M., Boutz, D. R., Bashyal, A., Refvik, S. T., Chiang, C.-M., Xhemalce, B., Paull, T. T., Brodbelt, J. S., Marcotte, E. M., & Miller, K. M. (2019). Systematic bromodomain protein screens identify homologous recombination and R-loop suppression pathways involved in genome integrity. *Genes & Development*, *33*(23–24), 1751–1774. https://doi.org/10.1101/gad.331231.119

Klages-Mundt, N. L., Kumar, A., Zhang, Y., Kapoor, P., & Shen, X. (2018). The Nature of Actin-Family Proteins in Chromatin-Modifying Complexes. *Frontiers in Genetics*, *9*, 398. https://doi.org/10.3389/fgene.2018.00398

Kokavec, J., Zikmund, T., Savvulidi, F., Kulvait, V., Edelmann, W., Skoultchi, A. I., & Stopka, T. (2017). The ISWI ATPase Smarca5 (Snf2h) Is Required for Proliferation and Differentiation of Hematopoietic Stem and Progenitor Cells. *Stem Cells (Dayton, Ohio)*, *35*(6), 1614–1623. https://doi.org/10.1002/stem.2604

Koludrovic, D., Laurette, P., Strub, T., Keime, C., Le Coz, M., Coassolo, S., Mengus, G., Larue, L., & Davidson, I. (2015). Chromatin-Remodelling Complex NURF Is Essential for Differentiation of Adult Melanocyte Stem Cells. *PLOS Genetics*, *11*(10), e1005555. https://doi.org/10.1371/journal.pgen.1005555

Koyauchi, T., Niida, H., Motegi, A., Sakai, S., Uchida, C., Ohhata, T., Iijima, K., Yokoyama, A., Suda, T., & Kitagawa, M. (2022). Chromatin-remodeling factor BAZ1A/ACF1 targets UV damage sites in an MLL1-

dependent manner to facilitate nucleotide excision repair. *Biochimica et Biophysica Acta (BBA) - Molecular Cell Research*, *1869*(11), 119332. https://doi.org/10.1016/j.bbamcr.2022.119332

Lalli, M. A., Jang, J., Park, J.-H. C., Wang, Y., Guzman, E., Zhou, H., Audouard, M., Bridges, D., Tovar, K. R., Papuc, S. M., Tutulan-Cunita, A. C., Huang, Y., Budisteanu, M., Arghir, A., & Kosik, K. S. (2016). Haploinsufficiency of BAZ1B contributes to Williams syndrome through transcriptional dysregulation of neurodevelopmental pathways. *Human Molecular Genetics*, *25*(7), 1294–1306. https://doi.org/10.1093/hmg/ddw010

Laurette, P., Coassolo, S., Davidson, G., Michel, I., Gambi, G., Yao, W., Sohier, P., Li, M., Mengus, G., Larue, L., & Davidson, I. (2020). Chromatin remodellers Brg1 and Bptf are required for normal gene expression and progression of oncogenic Braf-driven mouse melanoma. *Cell Death & Differentiation*, *27*(1), 29–43. https://doi.org/10.1038/s41418-019-0333-6

Lazzaro, M. A., & Picketts, D. J. (2001). Cloning and characterization of the murine *Imitation Switch* (ISWI) genes: Differential expression patterns suggest distinct developmental roles for Snf2h and Snf2l. *Journal of Neurochemistry*, *77*(4), 1145–1156. https://doi.org/10.1046/j.1471-4159.2001.00324.x

LeRoy, G., Loyola, A., Lane, W. S., & Reinberg, D. (2000). Purification and Characterization of a Human Factor That Assembles and Remodels Chromatin. *Journal of Biological Chemistry*, *275*(20), 14787–14790. https://doi.org/10.1074/jbc.C000093200

Li, Y., Gong, H., Wang, P., Zhu, Y., Peng, H., Cui, Y., Li, H., Liu, J., & Wang, Z. (2021). The emerging role of ISWI chromatin remodeling complexes in cancer. *Journal of Experimental & Clinical Cancer Research: CR*, *40*(1), 346. https://doi.org/10.1186/s13046-021-02151-x

Loyola, A., Huang, J.-Y., LeRoy, G., Hu, S., Wang, Y.-H., Donnelly, R. J., Lane, W. S., Lee, S.-C., & Reinberg, D. (2003). Functional Analysis of the Subunits of the Chromatin Assembly Factor RSF. *Molecular and Cellular Biology*, *23*(19), 6759–6768. https://doi.org/10.1128/MCB.23.19.6759-6768.2003

Marmorstein, R., & Zhou, M.-M. (2014). Writers and Readers of Histone Acetylation: Structure, Mechanism, and Inhibition. *Cold Spring Harbor Perspectives in Biology*, *6*(7), a018762–a018762. https://doi.org/10.1101/cshperspect.a018762

Min, S., Kim, K., Kim, S.-G., Cho, H., & Lee, Y. (2018). Chromatin-remodeling factor, RSF1, controls p53-mediated transcription in apoptosis upon DNA strand breaks. *Cell Death & Disease*, *9*(11), 1079. https://doi.org/10.1038/s41419-018-1128-2

Mittal, P., & Roberts, C. W. M. (2020). The SWI/SNF complex in cancer—Biology, biomarkers and therapy. *Nature Reviews. Clinical Oncology*, *17*(7), 435–448. https://doi.org/10.1038/s41571-020-0357-3

Mujtaba, S., Zeng, L., & Zhou, M.-M. (2007). Structure and acetyl-lysine recognition of the bromodomain. *Oncogene*, *26*(37), 5521–5527. https://doi.org/10.1038/sj.onc.1210618

Nakamura, Y., Umehara, T., Nakano, K., Jang, M. K., Shirouzu, M., Morita, S., Uda-Tochio, H., Hamana, H., Terada, T., Adachi, N., Matsumoto, T., Tanaka, A., Horikoshi, M., Ozato, K., Padmanabhan, B., & Yokoyama, S. (2007). Crystal Structure of the Human BRD2 Bromodomain. *Journal of Biological Chemistry*, *282*(6), 4193–4201. https://doi.org/10.1074/jbc.M605971200

Neigeborn, L., & Carlson, M. (1984). Genes affecting the regulation of SUC2 gene expression by glucose repression in Saccharomyces cerevisiae. *Genetics*, *108*(4), 845–858. https://doi.org/10.1093/genetics/108.4.845

Niri, F., Terpstra, A. N., Lim, K. R. Q., & McDermid, H. E. (2021). Chromatin remodeling factor CECR2 forms tissue-specific complexes with CCAR2 and LUZP1. *Biochemistry and Cell Biology*, *99*(6), 759–765. https://doi.org/10.1139/bcb-2021-0019

Norton, K. A., Niri, F., Weatherill, C. B., Williams, C. E., Duong, K., & McDermid, H. E. (2021). Implantation failure and embryo loss contribute to subfertility in female mice mutant for chromatin remodeler *Cecr2* †. *Biology of Reproduction*, *104*(4), 835–849. https://doi.org/10.1093/biolre/ioaa231

Oppikofer, M., Bai, T., Gan, Y., Haley, B., Liu, P., Sandoval, W., Ciferri, C., & Cochran, A. G. (2017). Expansion of the ISWI chromatin remodeler family with new active complexes. *EMBO Reports*, *18*(10), 1697–1706. https://doi.org/10.15252/embr.201744011

Oppikofer, M., Sagolla, M., Haley, B., Zhang, H.-M., Kummerfeld, S. K., Sudhamsu, J., Flynn, E. M., Bai, T., Zhang, J., Ciferri, C., & Cochran, A. G. (2017). Non-canonical reader modules of BAZ1A promote

recovery from DNA damage. *Nature Communications*, *8*(1), 862. https://doi.org/10.1038/s41467-017-00866-0

Pai, C., McIntosh, B. A., Knutsen, R. H., Levin, M. D., Tsang, K. M., Kozel, B. A., & Heuckeroth, R. O. (2024). Loss of Baz1b in mice causes perinatal lethality, growth failure, and variable multi-system outcomes. *Developmental Biology*, *505*, 42–57. https://doi.org/10.1016/j.ydbio.2023.09.007

Picketts, D., Mirzaa, G., Yan, K., Relator, R., Timpano, S., Yalcin, B., Collins, S., Ziegler, A., Pao, E., Oyama, N., Brischoux-Boucher, E., Piard, J., Monaghan, K., Sacoto, M. G., Dobyns, W., Park, K., Fernández-Mayoralas, D., Fernández-Jaén, A., Jayakar, P., … Sadikovic, B. (2023). *Pathogenic variants in SMARCA1 cause an X-linked neurodevelopmental disorder modulated by NURF complex composition* [Preprint]. In Review. https://doi.org/10.21203/rs.3.rs-3317938/v1

Poli, J., Gasser, S. M., & Papamichos-Chronakis, M. (2017). The INO80 remodeller in transcription, replication and repair. *Philosophical Transactions of the Royal Society of London. Series B, Biological Sciences*, *372*(1731), 20160290. https://doi.org/10.1098/rstb.2016.0290

Ren, J., Chen, Q.-C., Jin, F., Wu, H.-Z., He, M., Zhao, L., Yu, Z.-J., Yao, W.-F., Mi, X.-Y., Wang, E.-H., & Wei, M.-J. (2014). Overexpression of Rsf-1 correlates with pathological type, p53 status and survival in primary breast cancer. *International Journal of Clinical and Experimental Pathology*, *7*(9), 5595–5608.

Reyes, A. A., Marcum, R. D., & He, Y. (2021). Structure and Function of Chromatin Remodelers. *Journal of Molecular Biology*, *433*(14), 166929. https://doi.org/10.1016/j.jmb.2021.166929

Ribeiro-Silva, C., Vermeulen, W., & Lans, H. (2019). SWI/SNF: Complex complexes in genome stability and cancer. *DNA Repair*, *77*, 87–95. https://doi.org/10.1016/j.dnarep.2019.03.007

Ribeyre, C., Zellweger, R., Chauvin, M., Bec, N., Larroque, C., Lopes, M., & Constantinou, A. (2016). Nascent DNA Proteomics Reveals a Chromatin Remodeler Required for Topoisomerase I Loading at Replication Forks. *Cell Reports*, *15*(2), 300–309. https://doi.org/10.1016/j.celrep.2016.03.027

Roganowicz, M., Bär, D., Bersaglieri, C., Aprigliano, R., & Santoro, R. (2023). BAZ2A-RNA mediated association with TOP2A and KDM1A represses genes implicated in prostate cancer. *Life Science Alliance*, *6*(7), e202301950. https://doi.org/10.26508/lsa.202301950

Rolicka, A., Guo, Y., Gañez Zapater, A., Tariq, K., Quin, J., Vintermist, A., Sadeghifar, F., Arsenian-Henriksson, M., & Östlund Farrants, A. (2020). The chromatin-remodeling complexes B-WICH and NuRD regulate ribosomal transcription in response to glucose. *The FASEB Journal*, *34*(8), 10818–10834. https://doi.org/10.1096/fj.202000411R

Salvati, A., Melone, V., Sellitto, A., Rizzo, F., Tarallo, R., Nyman, T. A., Giurato, G., Nassa, G., & Weisz, A. (2022). Combinatorial targeting of a chromatin complex comprising Dot1L, menin and the tyrosine kinase BAZ1B reveals a new therapeutic vulnerability of endocrine therapy-resistant breast cancer. *Breast Cancer Research*, *24*(1), 52. https://doi.org/10.1186/s13058-022-01547-7

Scott, T. M., Guo, H., Eichler, E. E., Rosenfeld, J. A., Pang, K., Liu, Z., Lalani, S., Bi, W., Yang, Y., Bacino, C. A., Streff, H., Lewis, A. M., Koenig, M. K., Thiffault, I., Bellomo, A., Everman, D. B., Jones, J. R., Stevenson, R. E., Bernier, R., … Scott, D. A. (2020). *BAZ2B* haploinsufficiency as a cause of developmental delay, intellectual disability, and autism spectrum disorder. *Human Mutation*, *41*(5), 921–925. https://doi.org/10.1002/humu.23992

Sharif, S. B., Zamani, N., & Chadwick, B. P. (2021). BAZ1B the Protean Protein. *Genes*, *12*(10), 1541. https://doi.org/10.3390/genes12101541

Shen, X., Mizuguchi, G., Hamiche, A., & Wu, C. (2000). A chromatin remodelling complex involved in transcription and DNA processing. *Nature*, *406*(6795), 541–544. https://doi.org/10.1038/35020123

Shen, X., Ranallo, R., Choi, E., & Wu, C. (2003). Involvement of actin-related proteins in ATP-dependent chromatin remodeling. *Molecular Cell*, *12*(1), 147–155. https://doi.org/10.1016/s1097-2765(03)00264-8

Sheu, J. J.-C., Guan, B., Choi, J.-H., Lin, A., Lee, C.-H., Hsiao, Y.-T., Wang, T.-L., Tsai, F.-J., & Shih, I.-M. (2010). Rsf-1, a Chromatin Remodeling Protein, Induces DNA Damage and Promotes Genomic Instability. *Journal of Biological Chemistry*, *285*(49), 38260–38269. https://doi.org/10.1074/jbc.M110.138735

Shi, Y., Zhao, P., Dang, Y., Li, S., Luo, L., Hu, B., Wang, S., Wang, H., & Zhang, K. (2021). Functional roles of the chromatin remodeler SMARCA5 in mouse and bovine preimplantation embryos†. *Biology of Reproduction*, ioab081. https://doi.org/10.1093/biolre/ioab081

Singh, H. R., & Ladurner, A. G. (2014). ACF Takes the Driver's Seat. *Molecular Cell*, *55*(3), 345–346. https://doi.org/10.1016/j.molcel.2014.07.014

Spruijt, C. G., Gräwe, C., Kleinendorst, S. C., Baltissen, M. P. A., & Vermeulen, M. (2021). Cross-linking mass spectrometry reveals the structural topology of peripheral NuRD subunits relative to the core complex. *The FEBS Journal*, *288*(10), 3231–3245. https://doi.org/10.1111/febs.15650

Stanley, F. K. T., Moore, S., & Goodarzi, A. A. (2013). CHD chromatin remodelling enzymes and the DNA damage response. *Mutation Research*, *750*(1–2), 31–44. https://doi.org/10.1016/j.mrfmmm.2013.07.008

Stern, M., Jensen, R., & Herskowitz, I. (1984). Five SWI genes are required for expression of the HO gene in yeast. *Journal of Molecular Biology*, *178*(4), 853–868. https://doi.org/10.1016/0022-2836(84)90315-2

Tallant, C., Valentini, E., Fedorov, O., Overvoorde, L., Ferguson, F. M., Filippakopoulos, P., Svergun, D. I., Knapp, S., & Ciulli, A. (2015). Molecular Basis of Histone Tail Recognition by Human TIP5 PHD Finger and Bromodomain of the Chromatin Remodeling Complex NoRC. *Structure*, *23*(1), 80–92. https://doi.org/10.1016/j.str.2014.10.017

Tamkun, J. W., Deuring, R., Scott, M. P., Kissinger, M., Pattatucci, A. M., Kaufman, T. C., & Kennison, J. A. (1992). brahma: A regulator of Drosophila homeotic genes structurally related to the yeast transcriptional activator SNF2/SWI2. *Cell*, *68*(3), 561–572. https://doi.org/10.1016/0092-8674(92)90191-e

Tariq, K., & Östlund Farrants, A.-K. (2021). Antagonising Chromatin Remodelling Activities in the Regulation of Mammalian Ribosomal Transcription. *Genes*, *12*(7), 961. https://doi.org/10.3390/genes12070961

Thompson, P. J., Norton, K. A., Niri, F. H., Dawe, C. E., & McDermid, H. E. (2012). CECR2 Is Involved in Spermatogenesis and Forms a Complex with SNF2H in the Testis. *Journal of Molecular Biology*, *415*(5), 793–806. https://doi.org/10.1016/j.jmb.2011.11.041

Torchy, M. P., Hamiche, A., & Klaholz, B. P. (2015). Structure and function insights into the NuRD chromatin remodeling complex. *Cellular and Molecular Life Sciences*, *72*(13), 2491–2507. https://doi.org/10.1007/s00018-015-1880-8

Tyagi, M., Imam, N., Verma, K., & Patel, A. K. (2016). Chromatin remodelers: We are the drivers!! *Nucleus (Austin, Tex.)*, *7*(4), 388–404. https://doi.org/10.1080/19491034.2016.1211217

Tyutyunyk-Massey, L., Sun, Y., Dao, N., Ngo, H., Dammalapati, M., Vaidyanathan, A., Singh, M., Haqqani, S., Haueis, J., Finnegan, R., Deng, X., Kirberger, S. E., Bos, P. D., Bandyopadhyay, D., Pomerantz, W. C. K., Pommier, Y., Gewirtz, D. A., & Landry, J. W. (2021). Autophagy-Dependent Sensitization of Triple-Negative Breast Cancer Models to Topoisomerase II Poisons by Inhibition of the Nucleosome Remodeling Factor. *Molecular Cancer Research*, *19*(8), 1338–1349. https://doi.org/10.1158/1541-7786.MCR-20-0743

Wiechens, N., Singh, V., Gkikopoulos, T., Schofield, P., Rocha, S., & Owen-Hughes, T. (2016). The Chromatin Remodelling Enzymes SNF2H and SNF2L Position Nucleosomes adjacent to CTCF and Other Transcription Factors. *PLOS Genetics*, *12*(3), e1005940. https://doi.org/10.1371/journal.pgen.1005940

Wiles, E. T., Mumford, C. C., McNaught, K. J., Tanizawa, H., & Selker, E. U. (2022). The ACF chromatin-remodeling complex is essential for Polycomb repression. *eLife*, *11*, e77595. https://doi.org/10.7554/eLife.77595

Yip, D. J., Corcoran, C. P., Alvarez-Saavedra, M., DeMaria, A., Rennick, S., Mears, A. J., Rudnicki, M. A., Messier, C., & Picketts, D. J. (2012). Snf2l Regulates Foxg1-Dependent Progenitor Cell Expansion in the Developing Brain. *Developmental Cell*, *22*(4), 871–878. https://doi.org/10.1016/j.devcel.2012.01.020

Zaghlool, A., Halvardson, J., Zhao, J. J., Etemadikhah, M., Kalushkova, A., Konska, K., Jernberg-Wiklund, H., Thuresson, A., & Feuk, L. (2016). A Role for the Chromatin-Remodeling Factor *BAZ1A* in Neurodevelopment. *Human Mutation*, *37*(9), 964–975. https://doi.org/10.1002/humu.23034

Zahid, H., Buchholz, C. R., Singh, M., Ciccone, M. F., Chan, A., Nithianantham, S., Shi, K., Aihara, H., Fischer, M., Schönbrunn, E., Dos Santos, C. O., Landry, J. W., & Pomerantz, W. C. K. (2021). New Design Rules for Developing Potent Cell-Active Inhibitors of the Nucleosome Remodeling Factor (NURF) via BPTF

Bromodomain Inhibition. *Journal of Medicinal Chemistry*, *64*(18), 13902–13917. https://doi.org/10.1021/acs.jmedchem.1c01294

Zhou, Y. (2002). The chromatin remodeling complex NoRC targets HDAC1 to the ribosomal gene promoter and represses RNA polymerase I transcription. *The EMBO Journal*, *21*(17), 4632–4640. https://doi.org/10.1093/emboj/cdf460

Zikmund, T., Kokavec, J., Turkova, T., Savvulidi, F., Paszekova, H., Vodenkova, S., Sedlacek, R., Skoultchi, A. I., & Stopka, T. (2019). ISWI ATPase Smarca5 Regulates Differentiation of Thymocytes Undergoing β-Selection. *The Journal of Immunology*, *202*(12), 3434–3446. https://doi.org/10.4049/jimmunol.1801684

Zikmund, T., Paszekova, H., Kokavec, J., Kerbs, P., Thakur, S., Turkova, T., Tauchmanova, P., Greif, P. A., & Stopka, T. (2020). Loss of ISWI ATPase SMARCA5 (SNF2H) in Acute Myeloid Leukemia Cells Inhibits Proliferation and Chromatid Cohesion. *International Journal of Molecular Sciences*, *21*(6), 2073. https://doi.org/10.3390/ijms21062073

Zillner, K., Filarsky, M., Rachow, K., Weinberger, M., Längst, G., & Németh, A. (2013). Large-scale organization of ribosomal DNA chromatin is regulated by Tip5. *Nucleic Acids Research*, *41*(10), 5251–5262. https://doi.org/10.1093/nar/gkt218